Main manuscript

Title

Volcanic deposits select for woodiness on islands

Authors

Simon Biedermann[1,*], Frederic Lens[2,3], Nicolai M. Nürk[4,5], Carl Beierkuhnlein[1,5,6,7]

*Corresponding Author: Simon Biedermann, simon.biedermann@uni-bayreuth.de

Author Affiliations

1 Dept. of Biogeography, University of Bayreuth, Universitätsstr. 30, 95440 Bayreuth, Germany

2 Naturalis Biodiversity Center, PO Box 9517, 2300 RA Leiden, The Netherlands

3 Leiden University, Institute of Biology Leiden, Plant Sciences, Sylviusweg 72, 2333 BE Leiden, The Netherlands

4 Plant Systematics, Universitätsstr. 30, 95440 Bayreuth, Germany

5 Bayreuth Center of Ecology and Environmental Research BayCEER, Universitätsstr. 30, 95440 Bayreuth, Germany

6 Geographical Institute Bayreuth GIB, Universitätsstr. 30, 95440 Bayreuth, Germany

7 Departamento de Botánica, Universidad de Granada, Avenida de Fuentenueva S/N 18071, Granada, Spain

Abstract

Oceanic islands' unique biodiversity often arises from woody plant radiations derived from non-woody continental ancestors. Since Darwin, various theories have tried to explain the evolution of woodiness on islands (insular woodiness). Recently, frequent volcanic activity and burial of vegetation by volcanic ash (tephra) depositions were linked to the abundance of woody species on islands. In a chronosequence of five tephra fields on the island of La Palma (Canary Islands), we found a trend towards woody growth form, providing first evidence that volcanism favors woody species. Endemic insular woody species prevail on young fields, whereas woody species with woody colonizers become dominant on older fields. High similarity in functional traits is detected between fields. This highlight that endemic insular woody species show increased colonization and establishment ability on extreme habitats after volcanic eruptions, illustrating acquired functional advantages of endemic lineages that evolved woodiness on islands and sheds light on the role of environmental filtering during evolution.

Main Text

Introduction

Islands make up only 5.3 % of terrestrial habitats but approximately 21 % of Earth's total plant species diversity is endemic to islands [1]. Oceanic islands – through repeated formation through volcanic processes, spatial isolation and dynamic geological histories – act as cradles and museums for biodiversity, promoting both rapid speciation and high endemism [1–3]. At the same time, their isolation, small population sizes and relatively fast geological turnover can turn them into "evolutionary graveyards" with increased extinction rates [3,4]. This constant reshuffling of taxonomic cards by idiosyncratic processes is why islands, and their ecosystems, are perceived as "evolutionary arenas" [3,5,6]. On islands, plants have repeatedly evolved characteristic traits – often referred to as "island syndromes" [7]. This indicates a selective convergence towards certain plant traits on islands globally [7–11]. All oceanic islands are comparable in terms of low geodiversity resulting from their volcanic origin, despite significant differences in climatic conditions [12–14]. Understanding the evolutionary drivers that result in island syndromes is crucial for global island biodiversity and its conservation.

The most striking global island syndrome in plants is the in-situ evolution of woodiness after the arrival of a non-woody (i.e., herbaceous) continental population that established on the island (insular woodiness), which happened independently in at least 175 lineages within angiosperms [15–17]. Insular woody species co-exist with two other types of woody island species that originate from woody ancestors: some of the woody island species descended from woody colonisers that belong to lineages that have always been woody (ancestral woody species on islands), and other woody island species belong to lineages that evolved their woodiness on nearby continents (derived woodiness on islands) [18].

The mechanisms driving the evolution of insular woodiness are, in contrast to other island syndromes [7], incompletely understood [15,16]. Several hypotheses have been put forward to explain insular woodiness, most of them without experimental evidence [19]: (a) competition: in vegetations with few trees and dense herbaceous populations, increased stem woodiness in these herbaceous populations allows for taller growth to capture more sunlight [20,21]; (b) promotion of outcrossing: plants in isolated, pollinator-poor islands require increased flowering time to allow cross pollination, which in turn favors plant longevity and stimulates woodiness [22,23]; (c) climatic stability: the buffering effect of the surrounding ocean enable frost-free temperatures, thereby promoting continuous growth [15,24]; (d) lack of herbivory: large native mammal herbivores are absent on isolated islands, meaning that herbaceous species are not removed by grazers, which again promotes continuous plant growth [15]; (e) drought tolerance: increased stem woodiness allows for better preservation of intact root-to-shoot water transport [18,25,26], and recently (f) burial avoidance: volcanic activity and consequential burial of smaller, herbaceous plants by tephra selects for taller (insular, derived and ancestrally) woody plants to project over or penetrate through the volcanic depositions [27].

Volcanoes and their pyroclastic ejecta – especially tephra – can have strong impacts on vegetation [28–35]. Ecosystems close to an active crater are most strongly affected, as the thickness of the tephra layer increases towards the crater [29,32,33,36,37]. On every island with volcanic

activity, burial of plants smaller than the tephra layer has been occuring frequently over evolutionary time. This could be a selective process promoting taller, persistent, woody life forms and their functional traits, independent of their phylogenetic relatedness, indicating a true ecological selection [12,27,38–40].

According to the burial avoidance hypothesis [27], recurrent tephra deposits and the ecosystems they affect can be used as a model system to better understand why herbaceous lineages repeatedly evolved into insular woody species on volcanic archipelagoes. To test the burial avoidance hypothesis, we used a chronosequence of five tephra fields (54 – 6000 years old) on the island of La Palma (Canary Islands). We assessed whether the distinct evolutionary trajectories of woody island species (insular woody with herbaceous colonizer vs. woody island species with woody island colonizers) have a different impact on their burial survival and establishment in these extreme tephra habitats after volcanic eruptions.

We test the following assumptions predicted by the burial avoidance hypothesis:

(a) Woody species dominate plant communities on tephra fields as woody species are taller and more persistent than herbs and therefore better able to overcome burial by recurrent volcanic deposits.

(b) The predicted dominance of woody species on tephra fields is modulated by temporal and spatial factors irrespective of phylogenetic relatedness: we expect more woody species on younger fields (shorter time since eruption, meaning the selection for woody species by tephra occurred recently) and in areas closer to the crater (stronger impact of volcanic eruption with thicker tephra layer where only taller woody plants can overcome burial) than on older fields and areas further away.

(c) The higher occurrence of woody species and their associated traits according to the temporal and spatial pattern described in (b) should lead to a more constrained trait space on younger fields than on older fields.

Results

Woody species dominate, but their distribution changes with distinct evolutionary trajectories

In the 123 plots examined on five tephra fields on the island of La Palma, in total 38 plant species were recorded (Fig. 1a). Of these, 13 species are insular woody, 13 are woody species with woody colonizers and 12 are herbaceous (Supplement Table S1). Most species occur on only one tephra field. Each tephra field forms an individual plant community (Fig. 1b, Stress score = 0.104), with significant differences between the sites inferred by the overall analysis of similarities (ANOSIM, p = 9.99e-5, R = 0.543), and by pairwise ANOSIM comparisons (all p values < 0.0009, Supplement Table S2).

All tephra fields are dominated by woody species, with no significant trend in age (Kruskal-Wallis rank sum test, p = 0.104) (Figure 2a). Teneguia and Pico Birigoyo show a higher variance in the relative abundance of woody species, including more herbaceous species, but this is not significant (Kruskal-Wallis rank sum test, p = 0.104) (Figure 2b).

A significant shift in the relative abundance of insular woody species and woody species with woody colonizers is observed across the tephra fields (Kruskal-Wallis rank sum test, $p < 0.05$) (Figure 2c, d). The significant highest relative abundance of insular woody species is observed on the three youngest fields of Teneguia, Hoyo Negro, and San Antonio, and significantly drops on San Martin and especially on the oldest field of Pico Birigoyo. The relative abundance of woody species with woody colonizers shows the opposite pattern with age: on Teneguia, Hoyo Negro, and San Antonio almost no woody species with woody colonizers are observed, whereas their relative abundance significantly increases on San Martin and more particularly on Pico Birigoyo (Kruskal-Wallis rank sum test, $p < 0.05$).

Using regression analysis, the relative abundance of insular woody species significantly decreases with distance to the crater (p = 0.021, Nagelkerke Pseudo-R2 = 0.094), whereas the relative abundance of woody species with woody colonizers shows a significant opposite pattern (p = 0.043, Nagelkerke Pseudo-R2 = 0.068) (Supplement Fig. S1). The relative abundance of woody and herbaceous species does not show a pattern with distance to the crater (relative abundance of woody vs. herbaceous species: p = 0.385, Nagelkerke Pseudo-R2 = 0.0099).

On Teneguia, plots near the crater are almost exclusively dominated by insular woody species. By contrast, plots near the coast and far away from the crater show a higher abundance of herbs, explaining the highest variance in the relative abundance of insular woody species on this tephra field.

To understand the relative importance of abiotic predictors (age, distance to crater as a proxy for thickness of tephra deposition, and elevation) for relative abundance of plant growth forms, hierarchical partitioning was performed (Fig. 2e). Explained variance ranges between 37.6 % for the relative abundance of insular woody species and 3.6 % for woody / herbaceous species. The age of the tephra fields is the most important unique predictor for growth form: 3.3 % of explained variance for relative abundance of woody and herbaceous species, 20.9 % for insular woody species, and 14.1 % for other woody island species. Significance of predictors was

assessed using permutation tests (Supplement Table S3a). For relative abundance of woody and herbaceous species, age is the only significant predictor. For relative abundance of insular woody species and for other woody island species, age and distance to the crater are the only significant predictors.

Functional convergence across the tephra fields

Functional trait hypervolumes were constructed using a one-class support vector machine (SVM) learning model based on field measurements of plant height, leaf length, and length of reproductive unit (Fig. 3a). The occupied multidimensional space by the hypervolumes of the vegetation (functional richness) is highest on the oldest tephra field Pico Birigoyo and lowest on San Martin (Table 1). Functional dispersion level is similar for the five tephra fields and varies between 48.9 for the oldest Pico Birigoyo and 26.2 for the youngest Teneguia. Centroid location differs between the tephra fields. For leaf length, centroid location varies between 8.66 cm for San Martin and 3.31 cm for Hoyo Negro. For plant height, centroid location varies between 61.81 cm for Pico Birigoyo and 37.95 cm for Hoyo Negro. For length of the reproductive unit, centroid location varies between 12.1 mm for Hoyo Negro and 3.2 mm for San Martin.

Pairwise overlap of hypervolumes of the vegetation of the respective tephra fields was analyzed using Jaccard-Index as well as permutations. Pairwise overlap between the hypervolumes varies between 0.388 for the combination Pico Birigoyo and San Antonio, and 0.005 for the combination San Martin and Teneguia (Supplement Table S4, Supplement Fig. S2). Significant differences in the Jaccard Index between two hypervolumes (meaning that the two hypervolumes do not origin from a common trait probability function) is observed for the combinations of Pico Birigoyo – Hoyo Negro, Pico Birigoyo – San Martin, Pico Birigoyo – Teneguia, Hoyo Negro – San Martin, San Martin – San Antonio, and San Martin – Teneguia.

Using Gaussian Kernel density estimation (KDE) as an alternative algorithm to estimate the hypervolumes, the findings are confirmed (Supplement Fig. S3, Supplement Table S5). Functional richness and dispersion are lowest on Hoyo Negro, both are highest on the oldest field of Pico Birigoyo. A higher overlap between the hypervolumes is observed in comparison to SVM-derived hypervolumes, however, all the differences in Jaccard index are significant (Supplement Table S6).

To assess the occupancy of the different hypervolumes in functional trait space, occupancy analysis was performed (Fig. 3b). Occupied functional trait space is to 57.8 % occupied by one hypervolume, 43 % are occupied by at least two hypervolumes (20.9 % occupied by two hypervolumes, 16.4 % by three hypervolumes, 4.7 % by four hypervolumes, and 0.1 % by all five hypervolumes). Using KDE hypervolumes, a higher overlap is observed: 46.3 % of trait space is occupied by one hypervolume, 53.7 % by at least two hypervolumes (12.3 % occupied by two hypervolumes, 17.1 % by three hypervolumes, 16.6 % by four hypervolumes, and 7.8 % by five hypervolumes). Vegetation of Pico Birigoyo and San Martin add unique trait combinations not detected in other fields.

On plot level, significant differences (Kruskal-Wallis rank sum test, $p < 0.05$) are observed for all functional diversity indices (Fig. 4a-e). For functional richness and functional dispersion,

no clear pattern emerges. For total functional beta diversity within one single tephra field, the youngest Teneguia and the oldest Pico Birigoyo have significantly the highest beta diversity. For total beta diversity between the fields and replacement beta diversity between the fields, no pattern is observable. Most of the total beta diversity between the fields is due to replacement and not due to gain or loss of species richness.

For functional richness, most of the explained variance is uniquely predicted by elevation (9.5 %). For functional dispersion, age best predicts the explained variance, but with a very low value (1 %). Distance to the crater is the most important predictor for total functional beta diversity (2.7 %) (Fig. 4f). For functional richness elevation is the only significant predictor, for function dispersion none of the predictors is significant, for total functional beta diversity it is distance to the crater (Supplement Table S3b).

Phylogenetically independent patterns

All the detected patterns occur independent of phylogenetic relatedness (Supplement Fig. S4a). Standard effect size (SES) of Mean Pairwise Distance (MPD) and Mean Nearest Taxon Distance (MNTD) was used to assess phylogenetic dispersion (Supplement Fig. S4b). Positive values significantly different from zero indicate phylogenetic overdispersion (species are more distantly related as expected by chance), whereas negative values significant different from zero indicate phylogenetic clustering (species are more closely related). SES of MPD varies between -2.84 for Hoyo Negro and 0.929 for Pico Birigoyo. SES of MNTD varies between -2.19 for San Martin and 1.26 for Pico Birigoyo. Significant SES are observed for SES MPD for Hoyo Negro (SES MPD = -2.84, $p = 0.012$) and for SES MNTD for San Martin (SES MNTD = -2.19, $p = 0.007$).

Discussion

Using a chronosequence of five tephra fields on the island of La Palma (54 – 6000 years old), we show for the first time that volcanic deposits select towards woodiness on islands as all studied tephra fields are dominated by woody species. Interestingly, the evolutionary origin of woody species changes on the studied tephra fields, which is determined predominately by the age of the tephra fields and the proximity to the crater: insular woody species (stemming from herbaceous ancestors) are significantly more abundant on younger tephra fields and in areas closer to the crater with thicker tephra depositions, whereas the other woody island species (stemming from woody colonizers) become the dominant woody growth form on older tephra fields and in areas further away from the crater. These results confirm our first hypothesis that woody species are selected by volcanic tephra deposits but reject our second hypothesis suggesting that the dominance of woody species depends on both temporal (more on younger fields) and spatial proximity to the eruption (more in areas closer to the crater).

Vegetation on the five tephra fields forms distinct plant communities. The occupied functional trait space based on original measurements of plant height, leaf length and length of the reproductive unit shows high overlap between the studied fields, with some unique trait combinations added by some craters. No trend in functional richness and functional dispersion is detected, indicating functional convergence and filtering for traits associated with woody growth. Consequently, our third hypothesis states that the trait space is more constraint because of the proposed temporal and spatial patterns can be rejected. Phylogenetic dispersion on tephra field level is mostly statistically indifferent from neutral dispersion, so neither phylogenetic clustering nor overdispersion are observed, indicating that the observed patterns in woody species abundances and their traits occur independently of phylogenetic relatedness – likely reflecting an ecological selection for these, in addition to the rampant number of evolutionary shifts towards insular woodiness on the Canary Islands, and the fact that woody species with woody colonizers are common in many distantly related families [17,41,42].

Our findings highlight the strong abiotic filtering of volcanic tephra depositions towards woody species and their traits independent of phylogenetic origin. Shrubs constitute the bulk of woody species and can dominate succession on barren ground (primary succession) [43–45]. Generally, the repeated burial of vegetation by tephra should favor the woody growth form, irrespective of evolutionary origin [27]. Interestingly, at young fields and areas close to the crater, where the tephra layer may be so deep that the whole vegetation and its seed bank is covered, and dispersal of new seeds is needed for vegetation re-establishment [30,35,46,47], insular woody species dominate. One option to explain this is that insular woody species exhibit an increasing colonization and establishment ability on freshly deposited tephra, as we did not observe any species penetrating through the deep tephra layers at sites close to the crater. In contrast, on older plots and areas further away from the crater, woody species with woody colonizers become dominating and herbs occur, indicating weaker abiotic filtering at shallow deposits and increasing importance of seed sources in the vicinity, as even shallow tephra layers can remove the seed bank [35,47].

Priority effects may explain differences in community composition [48], in addition to the potential differences in colonization ability among woody species with a distinct evolutionary history. Under initial conditions with strong abiotic filtering and limited niches, early arriving, insular woody species – which their potentially higher establishing potential on fresh tephra – can occupy the few available niches rapidly after volcanic eruption and prevent later arriving species from establishing as niche overlap is expected between species [48,49]. As soil conditions ameliorate, woody species stemming from woody island colonizers may be able to enter the system.

Despite the distinct community composition across the studied tephra fields, functional trait overlap is high, without a trend in functional richness or functional dispersion over > 6000 years of succession – indicating functional convergence due to persistent abiotic filtering for woody species and their traits. These findings contrast with ecological theory also observed on islands, that predicts that trait convergence is expected in early successional communities due to abiotic filtering (only certain traits are able to establish), and trait divergence becomes important in later successional communities due to increasing importance of biotic interactions (facilitation and competition, which can lead to the exclusion of functionally similar species) [40,43,50–61]. Therefore, we would expect a constrained functional trait space in some of the younger fields as in young volcanic ecosystems with poor, initial soils, strong abiotic filtering should prevail, and a transition to trait divergence with age (as seen on La Palma's lava flows), which we do not observe [15,57,58,62–64]. This discrepancy may be due to persistent strong abiotic filtering for woody species and their traits. Schrader et al. [58] hypothesized that all islands filter towards early-successional establishment strategies (in addition to dispersal filters), which would in turn lead to functional convergence [15]. This filter may be frequent tephra depositions.

The unexpected outcomes of the functional traits space analyses may be due to the selection of measurements recorded in the field. We focused on easy-to-score traits which cover different axes in the plant functional spectrum (plant growth form, plant height, length of leaves (as a proxy for leaf area), and length of the reproductive unit) during our field work campaigns to cover as many plots as possible [54,65,66].

We find that abiotic filtering and priority effects jointly shape community and trait assemblage on these tephra fields. The observed trait convergence is independent from community composition if trait assemblage occurs due to deterministic assembly rules and differences in community composition are due to priority effects [48,49]. This may explain why individual tephra fields perform highly individual successional stabilities as well in terms of endemism, woodiness, and plant functional traits. Tephra fields can be seen as "smoking gun" ecosystems for the frequent habitat destruction and creation on oceanic islands. The frequent, recurring filtering through tephra depositions, initial habitat creation and colonization throughout evolutionary history can filter for certain traits and plant strategies associated with woody growth forms [39,65], which could explain why islands proportionally harbor more woody species than nearby continents.

Conclusion

On the five tephra fields investigated on the island of La Palma (50 - 6000 years old), a high abundance of woody species is observed, irrespective of the distance to the crater and age. Interestingly, the distinct evolutionary trajectories of the woody island species, either originating from an herbaceous (insular woody) or woody island colonizer, impact the location of the woody species and is best determined by the age of the tephra fields along with distance to the volcanic crater. Younger tephra fields and areas closer to the crater are significantly more occupied by insular woody species, whereas the other woody island species dominate older fields and areas further away from the crater. Unexpectedly, a high functional convergence is observed based on the traits scored in the field, suggesting a strong selection of volcanic activity and tephra depositions towards woody species and their associated traits. These patterns occur independently of phylogenetic relatedness.

Why insular woody species predominate on the initial, highly disturbed tephra sites remains unanswered. It could be due to an increased colonization and establishment ability of these species in comparison to the other woody and herbaceous island species, but the traits driving these differences are not known. Including additional traits, including also below-ground traits, may reveal differences in functional trait space that could explain why insular and other woody island species behave differently in the five tephra fields studied. Research on the drivers of community and trait assemblage is needed to better understand why tephra fields are unique in their community composition and similar in their trait composition. This would also directly link to one of the questions already posed by Darwin [22] why species became woody on islands. Tephra fields may be a good model system to provide answers to one of the most conspicuous aspects of insular floras. Understanding the global extent of tephra fields and its vegetation patterns may be crucial for a better understanding of the unique woody biodiversity on volcanic islands across the world.

Methods

Study site

All field data was recorded on the island of La Palma, Canary Islands, Spain. La Palma is located at the northwestern edge of the Canary Islands archipelago and can be divided into an older part in the north (ca. 2.0 Ma) as well as a younger part in the south (ca. 0.54 Ma) [54]. Besides El Hierro, La Palma is the only island of the Canary Islands at present in the juvenile shield stage and is the most active of the archipelago due to continuous eruptions [13,38]. In contrast to the northern part of the island, volcanism is still very active today in the south. Numerous eruptions were recorded in recent centuries (1585, 1646, 1677, 1712, 1949 and 1971), the last one occurring in 2021 [33,67,68]. La Palma is characterized by its subtropical-Mediterranean climate, which leads to humid winters and dry summers [69]. The study sites are located in the sunnier and drier southern half of the island which are influenced by high solar radiation.

The plots (n = 123) are located on the southern Cumbre Vieja ridge on five different aged tephra fields (from North to South: Pico Birigoyo (4025 ± 2000 BC, n = 45), Hoyo Negro (1949, n = 32), San Martin (1646, n = 26), San Antonio (1677, n = 10), and Teneguia (1971, n = 10; Fig. 6)). All plots are located on the slopes of the respective crater to reduce the influence of more recent volcanic depositions.

Data acquisition and preparation

Field work took place in March to April 2023 and February to March 2024, which is the best period to study annual herbaceous plants [64]. We tried to cover the whole vegetation on the five tephra fields, meaning that sampling took place from the edge of the tephra field towards the crater. In this area, plots were distributed randomly [70]. Areas within 20 m distance to roads, hiking paths, and visible human disturbance were excluded. The plots had a size of 4 x 4 m. Within this area, plant species identities, abundance, and damage (e.g., due to wind throw or herbivory) were recorded. Slope (measured with SUUNTO PM-5/360 PC Clinometer), altitude above sea level (measured with Polar Pacer Pro), and geographic location (measured with Garmin Oregon 300) were recorded. Areas with slopes exceeding 30 ° were excluded due to safety reasons. On San Antonio, sampling was only possible on the eastern slopes. This may lead to an underestimation of the vegetation covering this specific tephra field. However, our distant observations on the excluded sites showed similar vegetation patterns around all craters, thereby validating that our sampling strategy did not bias our results.

Depth of the tephra layer could not be determined in the field as the tephra layers could not be differentiated by eye in the field and the slopes of craters were too steep to dig holes. We therefore used distance to the crater as a proxy for tephra depth, which is a valid estimation based on the strong correlation between distance and depth in several publications [29,32,33,37].

Plant functional traits of the vegetation were sampled in situ (following [71]). In 2023 trait sampling was conducted on Pico Birigoyo, Hoyo Negro, and San Martin, one year later we

performed field work on San Antonio and Teneguia. Growth form of the species (woody, herbaceous) was recorded in the field. Furthermore, plant height, leaf length, and length of the reproductive unit were recorded. These traits cover different axes in the plant functional spectrum [54,65,66]. For the flower length of Asteraceae species, we used ligule length of the ray flower as the analogue for single flower length. For *Pinus canariensis*,. For non-flowering plants, like *Pinus canariensis*, we used the length of the microsporangia of the male cone as the analogue for single flower length (length of the reproducing organ as an analogue to flower length). Removing conifers with their unique traits compared to angiosperms, such as needle-like leaves and reproductive cones, did not change the results.

Traits were collected from randomly chosen adult individuals for each species on plot level that did not display significant damage from herbivores or wind, had no dead plant parts, and offer a representative subsample of the community. In 2024 additional vegetation sampling was conducted on Pico Birigoyo, Hoyo Negro, and San Martin without trait sampling, however. For these additional plots, averages of the traits sampled in 2023 at the respective crater were used.

To assess which species are insular or ancestral woody, first, a literature survey was performed [17,18]. For the species where the woodiness status (ancestral / insular) could not be obtained from the literature, ancestral state estimations were performed (see Data analysis).

Data analysis

For 18 species it can be confirmed that they are insular or ancestral woody. For other species with unknown woodiness status, phylogenies and plant life forms (woody / herbaceous) were acquired from the literature and online herbaria (Supplement Methods).

The phylogenies were used to assess evolutionary trajectories of life-history strategies across the studied clades. For this, an ancestral state reconstruction – focusing on the phylogenetic positions of shifts from herbaceous to woody life histories within each group – was performed using the package "phytools" (Version: 1.5-1, function *make.simmap()*, [72]). Stochastic character mapping with a Markov Chain Monte Carlo (MCMC) algorithm was used to sample the transition rate Q and life form histories from the posterior probability distribution [73,74]. For each species 1,000 iterations of the MCMC sampling on the acquired phylogenies that include the species and the closest relatives from the continent were performed.

Differences in plant community composition on the different tephra fields were analysed using ordination. First, a Bray-Curtis dissimilarity was calculated [75] (function vegdist(), package "vegan", [76]). This was followed by a Non-metric Multidimensional Scaling (NMDS) using k = 2 dimensions and at least 1000 random starts (function metaMDS(), package "vegan", [76]). Data points were grouped to the respective aged tephra fields where they were sampled. We had to remove one plot (PB_027_2023) because this singularity would overshadow the ordination. On this plot, we recorded *Silene vulgaris* with an abundance of 17 individuals.

Phylogenetic dispersion was assessed on a Canary Island angiosperm phylogeny [77] (Supplement Methods). However, multiple species could not be included. We opted to add

these species using the V.PhyloMaker2 package [78], which may underestimate the true evolutionary relationships. *Pinus canariensis* as a conifer needed to be excluded from the analysis. This may underestimate the true phylogenetic dispersion. However, we assume that adding *Pinus canariensis* to the analysis would make the phylogenetic dispersion even more neutral, as it occurs on almost every tephra field and is distantly related to all other plant species recorded. First, pairwise distance between the tips of the tree were calculated (function *cophenetic.phylo()*, package "ape", [79]). Then, abundance weighted standard effect sizes of Mean Pairwise Distance (MPD) and Mean Nearest Taxon Distance (MNTD) were estimated using the independent swap algorithm with 1000 runs with 10000 iterations each (function ses.mpd() and ses.mntd(), package "picante", [80]).

To assess the differences between the communities on the tephra fields, an analysis of similarity (ANOSIM) was performed using 10,000 permutations (function anosim(), package "vegan", [76]). This was followed up by a pairwise multilevel comparison to assess which tephra field community differs significantly from others using 10,000 permutations and Bonferroni's p-value correction method (function anosim.pairwise(), package "vegan.ex").

Differences in relative abundances of woody, herbaceous, ancestral woody, and insular woody species with the age of the tephra fields were analysed using a Kruskal-Wallis rank-sum test with the function *kruskal.test()*. This was followed up by a post-hoc test (Dunn test, function *dunnTest()*, package "FSA", [81]). Furthermore, to assess the influence of distance from the crater on the relative abundance of life forms, univariate regressions were performed using Generalized Linear Models (GLM) (function *glm()*, family binomial).

To assess the functional diversity between the respective aged tephra fields, the functional trait space was calculated using the n-dimensional hypervolume algorithm in the "hypervolume" package [82,83]. For hypervolume calculations, maximum trait values are often used [54,84]. However, this neglects the displayed phenotypic plasticity in functional traits of a species between different sites. Therefore, we opted to use the mean values of sampled traits per plot to estimate the trait hypervolumes. If traits were or could not be sampled on plot level, mean values of the respective trait of the respective species on the respective tephra field were used.

The functional trait space occupied by the vegetation of the different tephra fields was quantified using a one-class support vector machine (SVM) and Gaussian kernel density estimation (KDE) (function *hypervolume_svm()*, *hypervolume_gaussian()*, package "hypervolume", [83]). 1,000 Monte Carlo points per data point were used.

For KDE, a quantile threshold was chosen, that ensured that 95 % of the estimated probability density was enclosed by the chosen boundaries [85]. To make the hypervolumes comparable, we used a fixed kernel density estimate bandwidth of 0.5 standard deviations of the functional traits [54,86].

SVM parameters (ν, γ) influence size and shape of the hypervolume and therefore, values were varied (following [82]) and chosen by visual examination of the resulting hypervolumes, paying attention to the wrap around data points and projection into negative trait space, and used for all tephra fields for comparability reasons [82]. The final parameters are $\nu = 0.01$ and $\gamma = 0.5$.

The two algorithms were compared visually. We opted to use the SVM-derived hypervolumes for comparison of occupied trait space between the tephra fields, as they offer a tighter fit to the data points and do not show a projection into negative trait space. All other analyses on tephra field level were conducted the SVM-derived hypervolumes. Hypervolumes were compared with the centroid location (function *get_centroid()*, package "hypervolume", [83]). The overlap between the hypervolumes for the different tephra fields (Jaccard-Index) was quantified using the functions *hypervolume_set()* and *hypervolume_overlap_statistics()* (package "hypervolume", [83]). To assess if the calculated hypervolumes stem from a common trait probability distribution, pairwise comparison of hypervolumes were permuted 1,000 times (function *hypervolume_permute()*, package "hypervolume", [83]), and overlap statistics were calculated using the *hypervolume_overlap_test()* function and the Jaccard-Index (package "hypervolume", [87]).

We additionally used the occupancy framework of functional trait space to assess the overlap between the hypervolumes of the different tephra fields. Occupancy represents the mean number of individuals occupying a given point in multidimensional space. Mean occupancy was calculated using the function *hypervolume_n_occupancy()* (package "hypervolume", [83]).

To assess functional diversity on plot level, for each plot a hypervolume was calculated using Gaussian kernel density estimations with the function *hypervolume_gaussian()* (package "hypervolume" [83,88]). Here we opted for the KDE hypervolumes as the computational costs for SVM hypervolumes on plot level were too high and we did not compare the different algorithms directly (plot level vs. tephra field level). For comparability reasons of the KDE hypervolumes on plot level, a fixed kernel bandwidth was used of 0.5 standard deviations (following [54,86]).

Three components of functional diversity, namely functional richness, functional dispersion, and functional beta diversity, were calculated on tephra field and plot level using the functions *kernel.alpha()*, *kernel.dispersion()*, and *kernel.beta()* (package "BAT", [89,90]). Functional richness is the total volume of trait space. Functional dispersion is a measure of how spread or dense the trait space is. Both measures were scaled between 0 and 1.

Functional beta diversity was computed as the pairwise comparisons of dissimilarities between communities. This was done for (a) only the plots in a specific tephra field, and (b) for all plots. We then calculated the mean dissimilarity of all comparisons of a community with the rest of the communities. We analyzed the total beta diversity, which reflects both the volume replacement and the loss / gain (richness differences), and the replacement beta diversity.

Differences in functional richness, functional dispersion, and functional beta diversity on plot level between the tephra fields were analyzed using a Kruskal-Wallis rank-sum test based on the function *kruskal.test*, followed up by a post-hoc test (Dunn test, function *dunnTest()*, package "FSA", [81]).

To assess the relative importance of abiotic predictors (age, distance to the crater, and height) on life form abundances and functional diversity metrices, hierarchical partitioning was performed using the function *rdacca.hp()* (package "rdacca.hp", [91]). The significance of the

predictors was assessed using permutation tests with the function *permu.hp()* (package "rdacca.hp", [91]).

Assessment of insular woodiness

To assess the abundance patterns of insular and ancestral woody species, first, ancestral state estimations for species with unknown woodiness status were performed. *Pterocephalus porphyranthus* Svent., 1969 is part of a woody subclade and its closest relatives on the continent (*Pterocephalus spathulatus*, *Pterocephalus depressus*, *Pterocephalus strictus*, *Pterocephalus perennis*, and *Pterocephalus frutescens*) are all woody, leading to a posterior probability for being a shrub of 0.975 and an herb of 0.025 at the node *P. porphyranthus – P. frutescens* (Supplement Fig. S5). Including the continental herbaceous *Scabiosa* clade and the herbaceous *Pterocephalus* species (*P. papposus*, *P. brevis*, and *P. pulverulentus*), this leads to a posterior probability of 0.075 for being a shrub and 0.925 for being a herb at the node *P. porphyranthus* and *P. papposus*, and a probability of 0.002 for being a shrub and 0.998 for being a herb at the node *P. porphyranthus – Scabiosa africana*. This indicates a derived woodiness of *P. porphyranthus* which likely evolved on the continent.

Euphorbia balsamifera is nested in a woody clade and its closest relatives on the continent (*E. larica, E. schefflera, E. smithii*) are all woody, leading to a posterior probability for being a shrub of 0.964 and an herb of 0.036 at the node *E. balsamifera – E. smithii* (Supplement Fig. S6). Evidently, *E. balsamifera* is derived woody also because of its wide range along continental coastlines.

For *Schizogyne sericea* the closest relatives on the continent (*Limbarda crithmoides*, *Pulicaria incisa*, *P. mauritanica*, *Jasonia tuberosa*) are all herbaceous. This leads to a posterior probability for being an herb of 0.877 and a shrub of 0.123 at the node *S. sericea – L. crithmoides* and a posterior probability of 0.802 (herb) and 0.198 (shrub) at the node *S. sericea – Lifago dielsii* (Supplement Fig. S7), indicating that *S. sericea* is insular woody. For *Schizogyne sericeae*, the outgroup sampling is poor in the phylogeny that was available [92].

Bystropogon origanifolius closest relatives from the continent are all herbaceous (*Acinos arvensis*, *Ziziphora clinopodioides*, *Clinopodium gracile*, *C. chinese, C. gracile*), leading to a posterior probability of 0.462 being a shrub and 0.538 being an herb at the node *B. origanifolius – C. gracile*. Including the New World Menthinae clade leads to a posterior probability of 0.521 being a shrub and 0.479 being an herb at the node New World Menthinae – *B. origanifolius* (Supplement Fig. S8). For *Bystropogon origanifolius* we used a phylogeny based on ITS and ETS sequences [93]. However, the phylogeny needs to be interpreted with caution as phylogenies inferred from nuclear and chloroplast DNA differ [93].

For *Polycarpaea divaricata* and *Polycarpaea arsitata* most of the closest relatives from the continent are woody (e.g., *Polycarpaea nivea*, *Pollichia campestris*, *Sphaerocoma hookeri*, *S. aucheri*; exception *Polycarpon prostratum* and *Polycarpaea filifolia*). This leads to a posterior lifeform probability of 0.998 being a shrub and 0.002 being an herb at the node *Sphaerocoma hookeri – Polycarpaea divaricata / aristata*. Including a broader part of the tree leads to a posterior probability of 0.998 being a shrub and 0.002 being an herb at the node *Polycarpon*

513 *suffruticosum – Polycarpaea divaricata / aristata*, indicating that these species are ancestrally
514 woody (Supplement Fig. S9).

515 Following a maximum parsimony approach and visual tracking of character evolution,
516 *Forsskaolea angustifolia* is classified as ancestrally woody. This was done as for this species
517 no phylogenetic tree could be obtained from the literature. Better resolved phylogenies may
518 alter the inferred character evolution.

519

References

1. Schrader, J. *et al.* Islands are key for protecting the world's plant endemism. *Nature* **634**, 868–874 (2024).

2. Kier, G. *et al.* A global assessment of endemism and species richness across island and mainland regions. *Proc. Natl. Acad. Sci.* **106**, 9322–9327 (2009).

3. Whittaker, R. J. *et al. Island Biogeography: Geo-Environmental Dynamics, Ecology, Evolution, Human Impact, and Conservation*. (Oxford University Press, Oxford, New York, 2023).

4. Fernández-Palacios, J. M. *et al.* Scientists' warning – the outstanding biodiversity of islands is in peril. *Glob. Ecol. Conserv.* **31**, e01847 (2021).

5. Nürk, N. M. *et al.* Diversification in evolutionary arenas — assessment and synthesis. *Ecol. Evol.* **10**, 6163–6182 (2020).

6. Beierkuhnlein, C. Speciation happens in company – not in isolation. *Npj Biodivers.* **3**, 1–7 (2024).

7. Losos, J. B. & Ricklefs, R. E. Adaptation and diversification on islands. *Nature* **457**, 830–836 (2009).

8. Shaw, K. L. & Gillespie, R. G. Comparative phylogeography of oceanic archipelagos: hotspots for inferences of evolutionary process. *Proc. Natl. Acad. Sci.* **113**, 7986–7993 (2016).

9. Crawford, D. J. & Archibald, J. K. Island floras as model systems for studies of plant speciation: prospects and challenges. *J. Syst. Evol.* **55**, 1–15 (2017).

10. Whittaker, R. J., Fernández-Palacios, J. M., Matthews, T. J., Borregaard, M. K. & Triantis, K. A. Island biogeography: taking the long view of nature's laboratories. *Science* **357**, eaam8326 (2017).

11. Baeckens, S. & Damme, R. V. The island syndrome. *Curr. Biol.* **30**, R338–R339 (2020).

12. Carracedo, J. C., Badiola, E. R., Guillou, H., Nuez, J. de la & Torrado, F. J. P. Geology and volcanology of La Palma and El Hierro, Western Canaries. *Estud. Geológicos* **57**, 175–273 (2001).

13. Hoernle, K. & Carracedo, J.-C. Canary Islands, Geology. in *Encyclopedia of Islands* (eds Gillespie, R. & Clague, D.) 133–143 (University of California Press, 2009). doi:10.1525/9780520943728-032.

14. Kienle, D. *et al.* Geodiversity and biodiversity on a volcanic island: the role of scattered phonolites for plant diversity and performance. *Biogeosciences* **19**, 1691–1703 (2022).

15. Carlquist, S. *Island Biology*. (Columbia University Press, New York, 1974). doi:10.5962/bhl.title.63768.

16. Burns, K. C. *Evolution in Isolation: The Search for an Island Syndrome in Plants*. (Cambridge University Press, Cambridge, 2019). doi:10.1017/9781108379953.

17. Zizka, A. *et al.* The evolution of insular woodiness. *Proc. Natl. Acad. Sci.* **119**, e2208629119 (2022).

18. Hooft van Huysduynen, A. *et al.* Temporal and palaeoclimatic context of the evolution of insular woodiness in the Canary Islands. *Ecol. Evol.* **11**, 12220–12231 (2021).

19. Lens, F., Davin, N., Smets, E. & del Arco, M. Insular woodiness on the Canary Islands: a remarkable case of convergent evolution. *Int. J. Plant Sci.* **174**, 992–1013 (2013).

20. Darwin, C. *The Origin of Species*. (John Murray, UK, 1859).

21. Givnish, T. J. Adaptive plant evolution on plants - classical patterns, molecular data, new insights. in *Evolution of Islands* (ed. Grant, P. R.) 281–304 (2001).

22. Wallace, A. R. *Tropical Nature, and Other Essays*. (Macmillan and co, London, 1878). doi:10.5962/bhl.title.1261.

23. Böhle, U. R., Hilger, H. H. & Martin, W. F. Island colonization and evolution of the insular woody habit in Echium L. (Boraginaceae). *Proc. Natl. Acad. Sci.* **93**, 11740–11745 (1996).

24. Carlquist, S. How wood evolves: a new synthesis. *Botany* **90**, 901–940 (2012).

25. Lens, F. *et al.* Embolism resistance as a key mechanism to understand adaptive plant strategies. *Curr. Opin. Plant Biol.* **16**, 287–292 (2013).

26. Dória, L. C. *et al.* Embolism resistance in stems of herbaceous Brassicaceae and Asteraceae is linked to differences in woodiness and precipitation. *Ann. Bot.* **124**, 1–14 (2019).

27. Beierkuhnlein, C. *et al.* Volcanic ash deposition as a selection mechanism towards woodiness. *Npj Biodivers.* **2**, 1–8 (2023).

28. del Moral, R., Titus, J. h. & Cook, A. m. Early primary succession on Mount St. Helens, Washington, USA. *J. Veg. Sci.* **6**, 107–120 (1995).

29. del Moral, R. & Grishin, S. Y. Volcanic disturbance and ecosystem recovery. in *Ecosystems of the World* (ed. Walker) 137–160 (1999).

30. Dale, V. H., Delago-Acevedo, J. & MacMahon, J. Effects of modern volcanic eruptions on vegetation. in *Volcanoes and their Environment* (eds Marti, J. & Ernst, G. G. J.) (Cambridge University Press, Cambridge, UK, 2005).

31. Efford, J., Clarkson, B. & Bylsma, R. Persistent effects of a tephra eruption (AD 1655) on treeline composition and structure, Mt Taranaki, New Zealand. *N. Z. J. Bot.* **52**, 245–261 (2014).

32. Dale, V. H., Swanson, F. J. & Crisafulli, C. M. Disturbance, survival, and sucession: understanding ecological repsonses to the 1980 eruption of Mt. St. Helens. in (eds Crisafulli, C. M. & Dale, V. H.) 3–12 (Springer, 2018).

33. Carracedo, J. C. *et al.* The 2021 eruption of the Cumbre Vieja volcanic ridge on La Palma, Canary Islands. *Geol. Today* **38**, 94–107 (2022).

34. Nogales, M. *et al.* The fate of terrestrial biodiversity during an oceanic island volcanic eruption. *Sci. Rep.* **12**, 19344 (2022).

35. Grishin, S. Yu., del Moral, R., Krestov, P. V. & Verkholat, V. P. Succession following the catastrophic eruption of Ksudach volcano (Kamchatka, 1907). *Vegetatio* **127**, 129–153 (1996).

36. Weiser, F. *et al.* Impact of volcanic sulfur emissions on the pine forest of La Palma, Spain. *Forests* **13**, 299 (2022).

37. Shatto, C. *et al.* Volcanic tephra deposition dataset based on interpolated field measurements following the 2021 Tajogaite eruption on La Palma, Canary Islands, Spain. *Data Brief* **52**, 109949 (2024).

38. Carracedo, J. Geological map of La Palma, Canary Islands. *Geol. Map* (2001).

39. Barajas Barbosa, M. P. *et al.* Assembly of functional diversity in an oceanic island flora. *Nature* **619**, 545–550 (2023).

40. Schrader, J. *et al.* Trait filtering in island floras: a conceptual framework. *J. Biogeogr.* **51**, 1596–1606 (2024).

41. Doyle, J. A. Molecular and fossil evidence on the origin of Angiosperms. *Annu. Rev. Earth Planet. Sci.* **40**, 301–326 (2012).

42. He, X. & Groover, A. T. The Genomics of Wood Formation in Angiosperm Trees. in *Comparative and Evolutionary Genomics of Angiosperm Trees* (eds Groover, A. & Cronk, Q.) 205–225 (Springer International Publishing, Cham, 2017). doi:10.1007/7397_2016_17.

43. Karadimou, E. *et al.* Functional diversity changes over 100 yr of primary succession on a volcanic island: insights into assembly processes. *Ecosphere* **9**, e02374 (2018).

44. Cabrera Rodríguez, F., Otto, R. & Fernández-Palacios, J. M. Changes in soil chemical properties and plant species composition during primary succession on an oceanic island. *J. Veg. Sci.* **33**, e13137 (2022).

45. del Moral, R. & Wood, D. M. Early primary succession on the volcano Mount St. Helens. *J. Veg. Sci.* **4**, 223–234 (1993).

46. Eggler, W. A. Plant life of Paricutin Volcano, Mexico, eight years after activity ceased. *Am. Midl. Nat.* **69**, 38–68 (1963).

47. Medina, F. M. *et al.* Seed bank and ashfalls: the ecological resetting effect of the recent Tajogaite Volcano eruption in the Canary pine forest (La Palma, Spain). *J. Veg. Sci.* **36**, e70045 (2025).

48. Fukami, T. Historical contingency in community assembly: integrating niches, species pools, and priority effects. *Annu. Rev. Ecol. Evol. Syst.* **46**, 1–23 (2015).

49. Vannette, R. L. & Fukami, T. Historical contingency in species interactions: towards niche-based predictions. *Ecol. Lett.* **17**, 115–124 (2014).

50. Callaway, R. M. & Walker, L. R. Competition and facilitation: a synthetic approach to interactions in plant communities. *Ecology* **78**, 1958–1965 (1997).

51. Grime, J. P. Trait convergence and trait divergence in herbaceous plant communities: mechanisms and consequences. *J. Veg. Sci.* **17**, 255–260 (2006).

52. Weiher, E. & Keddy, P. A. Assembly rules, null models, and trait dispersion: new questions from old patterns. *Oikos* **74**, 159–164 (1995).

53. Cornwell, W. K., Schwilk, L. D. W. & Ackerly, D. D. A trait-based test for habitat filtering: convex hull volume. *Ecology* **87**, 1465–1471 (2006).

54. Hanz, D. M. *et al.* Climatic and biogeographical drivers of functional diversity in the flora of the Canary Islands. *Glob. Ecol. Biogeogr.* **31**, 1313–1331 (2022).

55. Ratier Backes, A. *et al.* Mechanisms behind elevational plant species richness patterns revealed by a trait-based approach. *J. Veg. Sci.* **34**, e13171 (2023).

56. MacArthur, R. & Levins, R. The limiting similarity, convergence, and divergence of coexisting species. *Am. Nat.* **101**, 377–385 (1967).

57. Whittaker, R. J., Bush, M. B. & Richards, K. Plant recolonization and vegetation succession on the Krakatau Islands, Indonesia. *Ecol. Monogr.* **59**, 59–123 (1989).

58. Schrader, J., Wright, I. J., Kreft, H. & Westoby, M. A roadmap to plant functional island biogeography. *Biol. Rev.* **96**, 2851–2870 (2021).

59. Whittaker, R. J., Jones, S. H. & Partomihardjo, T. The rebuilding of an isolated rain forest assemblage: how disharmonicis the flora of Krakatau? *Biodivers. Conserv.* **6**, 1671–1696 (1997).

60. Ulrich, W., Zaplata, M. K., Winter, S. & Fischer, A. Spatial distribution of functional traits indicates small scale habitat filtering during early plant succession. *Perspect. Plant Ecol. Evol. Syst.* **28**, 58–66 (2017).

61. Wilfahrt, P. A., Collins, B. & White, P. S. Shifts in functional traits among tree communities across succession in eastern deciduous forests. *For. Ecol. Manag.* **324**, 179–185 (2014).

62. Carvajal-Endara, S., Hendry, A. P., Emery, N. C. & Davies, T. J. Habitat filtering not dispersal limitation shapes oceanic island floras: species assembly of the Galápagos archipelago. *Ecol. Lett.* **20**, 495–504 (2017).

63. Aikio, S., Ramula, S., Muola, A. & von Numers, M. Island properties dominate species traits in determining plant colonizations in an archipelago system. *Ecography* **43**, 1041–1051 (2020).

64. Otto, R. *et al.* Primary succession and plant functional traits on an oceanic island. *J. Ecol.* **113**, 1475–1490 (2025).

65. Laughlin, D. C. Unifying functional and population ecology to test the adaptive value of traits. *Biol. Rev.* **99**, 1976–1991 (2024).

66. Westoby, M. A leaf-height-seed (LHS) plant ecology strategy scheme. *Plant Soil* **199**, 213–227 (1998).

67. White, J. D. L. & Schmincke, H.-U. 1949 eruption on La Palma Canary Islands. *J. Volcanol. Geotherm. Res.* **94**, 283–304 (1999).

68. Longpré, M.-A. & Felpeto, A. Historical volcanism in the Canary Islands; Part 1: a review of precursory and eruptive activity, eruption parameter estimates, and implications for hazard assessment. *J. Volcanol. Geotherm. Res.* **419**, 107363 (2021).

69. Irl, S. D. H. *et al.* Climate vs. topography – spatial patterns of plant species diversity and endemism on a high-elevation island. *J. Ecol.* **103**, 1621–1633 (2015).

70. Schweiger, A. H., Irl, S. D. H., Steinbauer, M. J., Dengler, J. & Beierkuhnlein, C. Optimizing sampling approaches along ecological gradients. *Methods Ecol. Evol.* **7**, 463–471 (2016).

71. Pérez-Harguindeguy, N. *et al.* New handbook for standardised measurement of plant functional traits worldwide. https://hdl.handle.net/11299/177647 (2013).

72. Revell, L. J. phytools: an R package for phylogenetic comparative biology (and other things). *Methods Ecol. Evol.* **3**, 217–223 (2012).

73. Huelsenbeck, J. P., Nielsen, R. & Bollback, J. P. Stochastic mapping of morphological characters. *Syst. Biol.* **52**, 131–158 (2003).

74. Revell, L. J. & Harmon, L. J. *Phylogenetic Comparative Methods in R*. (Princeton University Press, Princeton ; Oxford, 2022).

75. Bray, J. R. & Curtis, J. T. An ordination of the upland forest communities of Southern Wisconsin. *Ecol. Monogr.* **27**, 325–349 (1957).

76. Oksanen, J. *et al.* vegan: Community Ecology Package. (2024).

77. Brewer, R. F. A. *et al.* Trait-dependent diversification and spatio-ecological limits drive angiosperm diversity unevenness across the Canary Islands archipelago. 2025.09.19.677265 Preprint at https://doi.org/10.1101/2025.09.19.677265 (2025).

78. Jin, Y. & Qian, H. V.PhyloMaker2: an updated and enlarged R package that can generate very large phylogenies for vascular plants. *Plant Divers.* **44**, 335–339 (2022).

79. Paradis, E. *et al.* ape: Analyses of Phylogenetics and Evolution. (2024).

80. Kembel, S. W. *et al.* Picante: R tools for integrating phylogenies and ecology. *Bioinformatics* **26**, 1463–1464 (2010).

81. Ogle, D. H., Doll, J. C., Wheeler, A. P., & Dinno, A. FSA: Simple Fisheries Stock Assessment Methods. (2023).

82. Blonder, B. Hypervolume concepts in niche- and trait-based ecology. *Ecography* **41**, 1441–1455 (2018).

83. Blonder, B. *et al.* hypervolume: High Dimensional Geometry, Set Operations, Projection, and Inference Using Kernel Density Estimation, Support Vector Machines, and Convex Hulls. (2024).

84. Cutts, V. *et al.* Scientific floras can be reliable sources for some trait data in a system with poor coverage in global trait databases. *J. Veg. Sci.* **32**, e12996 (2021).

85. Blonder, B., Lamanna, C., Violle, C. & Enquist, B. J. The n-dimensional hypervolume. *Glob. Ecol. Biogeogr.* **23**, 595–609 (2014).

86. Lamanna, C. *et al.* Functional trait space and the latitudinal diversity gradient. *Proc. Natl. Acad. Sci.* **111**, 13745–13750 (2014).

87. Chen, D., Laini, A. & Blonder, B. W. Statistical inference methods for n-dimensional hypervolumes: applications to niches and functional diversity. *Methods Ecol. Evol.* **15**, 657–665 (2024).

720 88. Laini, A., Datry, T. & Blonder, B. W. N-dimensional hypervolumes in trait-based
721 ecology: does occupancy rate matter? *Funct. Ecol.* **37**, 1802–1814 (2023).

722 89. Cardoso, P., Rigal, F. & Carvalho, J. C. BAT – Biodiversity Assessment Tools, an R
723 package for the measurement and estimation of alpha and beta taxon, phylogenetic
724 and functional diversity. *Methods Ecol. Evol.* **6**, 232–236 (2015).

725 90. Mammola, S. & Cardoso, P. Functional diversity metrics using kernel density n-
726 dimensional hypervolumes. *Methods Ecol. Evol.* **11**, 986–995 (2020).

727 91. Lai, J., Zou, Y., Zhang, J. & Peres-Neto, P. R. Generalizing hierarchical and
728 variation partitioning in multiple regression and canonical analyses using the rdacca.hp
729 R package. *Methods Ecol. Evol.* **13**, 782–788 (2022).

730 92. Francisco-Ortega, J., Park, S.-J., Santos-guerra, A., Benabid, A. & Jansen, R. K.
731 Origin and evolution of the endemic Macaronesian Inuleae (Asteraceae): evidence from
732 the internal transcribed spacers of nuclear ribosomal DNA. *Biol. J. Linn. Soc.* **72**, 77–97
733 (2001).

734 93. Drew, B. T., Liu, S., Bonifacino, J. M. & Sytsma, K. J. Amphitropical disjunctions in
735 New World Menthinae: three Pliocene dispersals to South America following late
736 Miocene dispersal to North America from the Old World. *Am. J. Bot.* **104**, 1695–1707
737 (2017).

Acknowledgements

Hypervolume permutations were performed using the festus-cluster of the Bayreuth Centre for High Performance Computing (https://www.bzhpc.uni-bayreuth.de), funded by the Deutsche Forschungsgemeinschaft (DFG, German Research Foundation) - 523317330.

We especially thank Anna Hollweg, Anna-Maria Seiverth, Lena Wege, and Trevor Roberts for their support during the field work, and Lilli Oberdörffer for proof-reading.

Author contributions

Conceptualization: SB, CB; Field work, data curation, formal analysis: SB; Methodology: SB, FL, NMN, CB; Writing – Original draft: SB; Writing – Rewiew & Editing: SB, FL, NMN, CB.

Competing interests

-

Materials & Correspondence

All correspondence should be addressed to Simon Biedermann: simon.biedermann@uni-bayreuth.de

All data and code will be made publicly available.

Tables

Table 1. Functional diversity indices and centroid location of the hypervolumes of the vegetation of the five tephra fields estimated using one-class support vector machine (SVM) learning model.

Tephra field	Functional richness	Functional dispersion	Centroid location – Leaf length [cm]	Centroid location – Plant height [cm]	Centroid location – Length reproductive unit [mm]
Pico Birigoyo	9994.8	48.9	3.76	61.81	8.8
Hoyo Negro	2891.4	27.7	3.31	37.95	12.1
San Martin	644.0	47.3	8.66	59.54	3.2
San Antonio	8879.8	35.0	5.96	46.95	9.2
Teneguia	2628.0	26.2	4.49	55.82	8.9

Figures

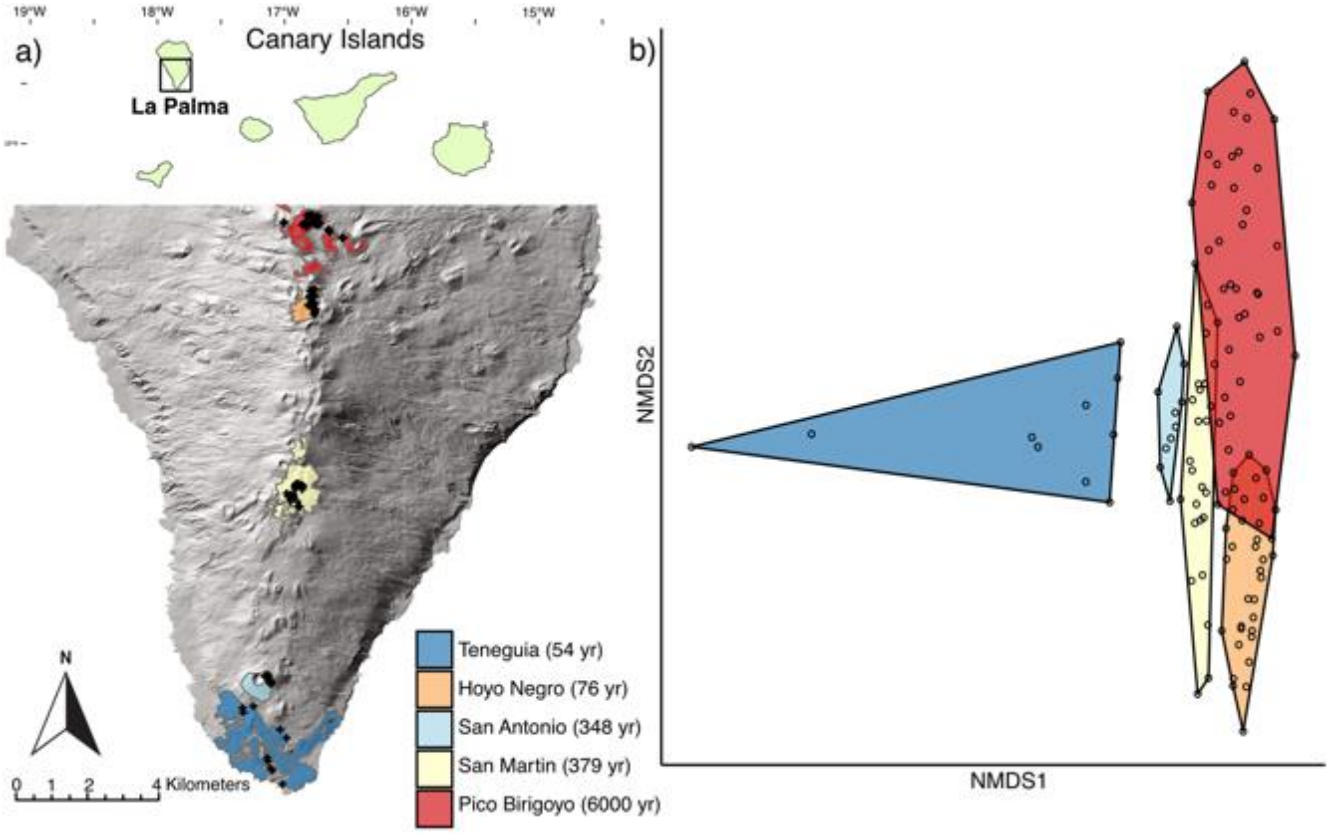

Figure 1. Study area and plant community composition. (a) Overview of the study area on the southern part of La Palma, Spain, its location within the Canary archipelago (Spain) and plot distribution within the five different tephra fields along the Cumbre Vieja ridge in the southern part of La Palma. The extent of the tephra fields is associated with the eruption of a specific crater and time since the last eruption. (b) Differences in plant community composition of the five tephra fields analyzed using Non-metric Multidimensional Scaling (NMDS) (Stress score = 0.104). Each tephra field forms its own unique community, with only marginal overlap.

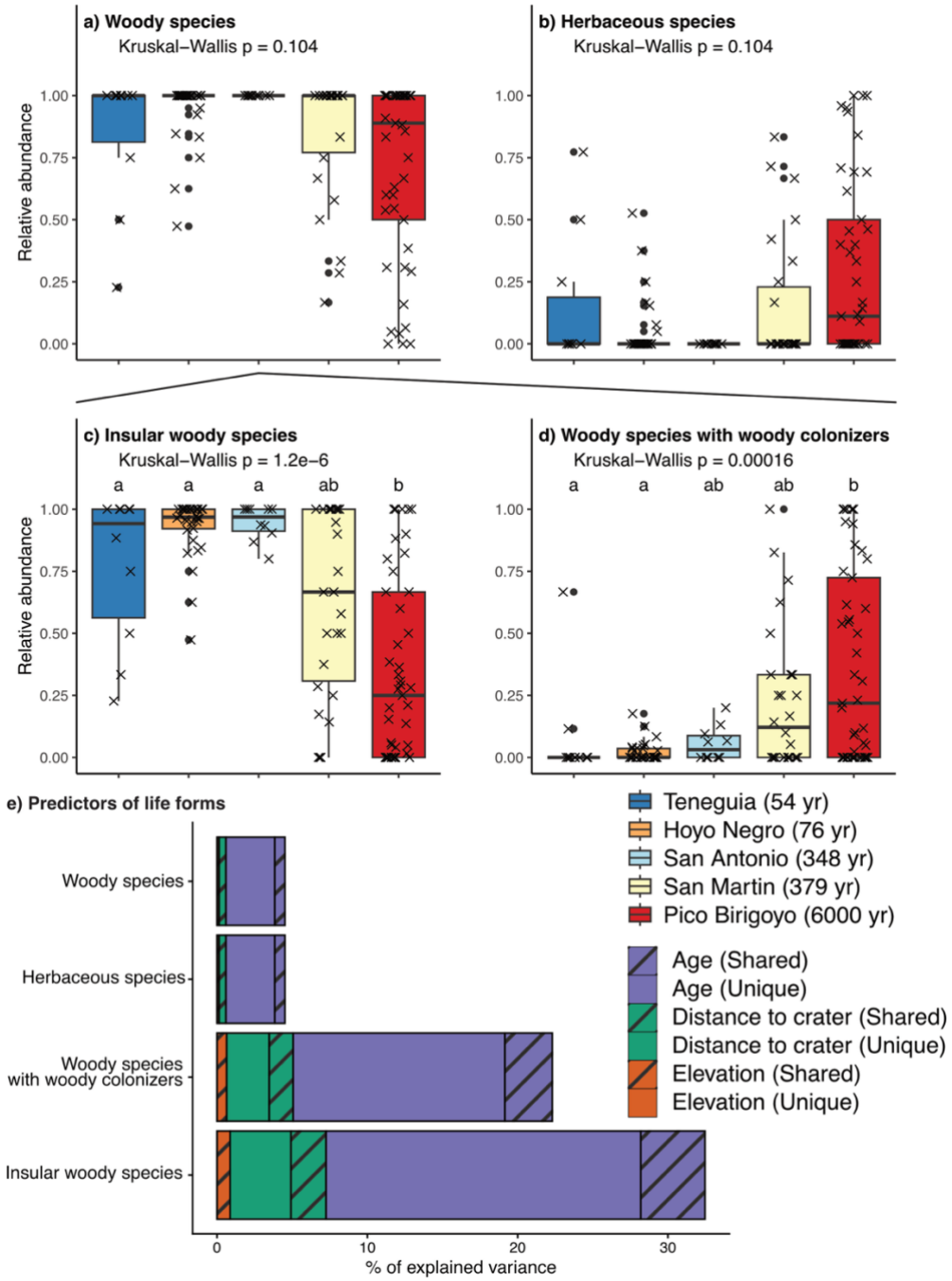

773

774 **Figure 2.** Abundance patterns of different life forms on the five tephra fields of La Palma. (a)
775 Relative abundance of woody species shows that all tephra fields are dominated by woody
776 species, with no significant differences between them. (b) Relative abundance of herbaceous
777 species, demonstrating that herbs are almost absent on the tephra fields. (c) Relative abundance
778 of insular woody species. Younger tephra fields (meaning less time since eruption) are
779 dominated by insular woody species, whereas this dominance gradually decreases with age. (d)
780 Relative abundance of woody species evolved from woody island colonizers. On younger
781 craters, these woody species are almost absent, but their relative abundance increases with the
782 age of the tephra fields. (e) Relative contribution in abiotic predictors in explaining the

observed variance in the relative abundance of life forms. Note that the unique (solid) and average shared (dashed) explained variance represent adjusted R^2 values.

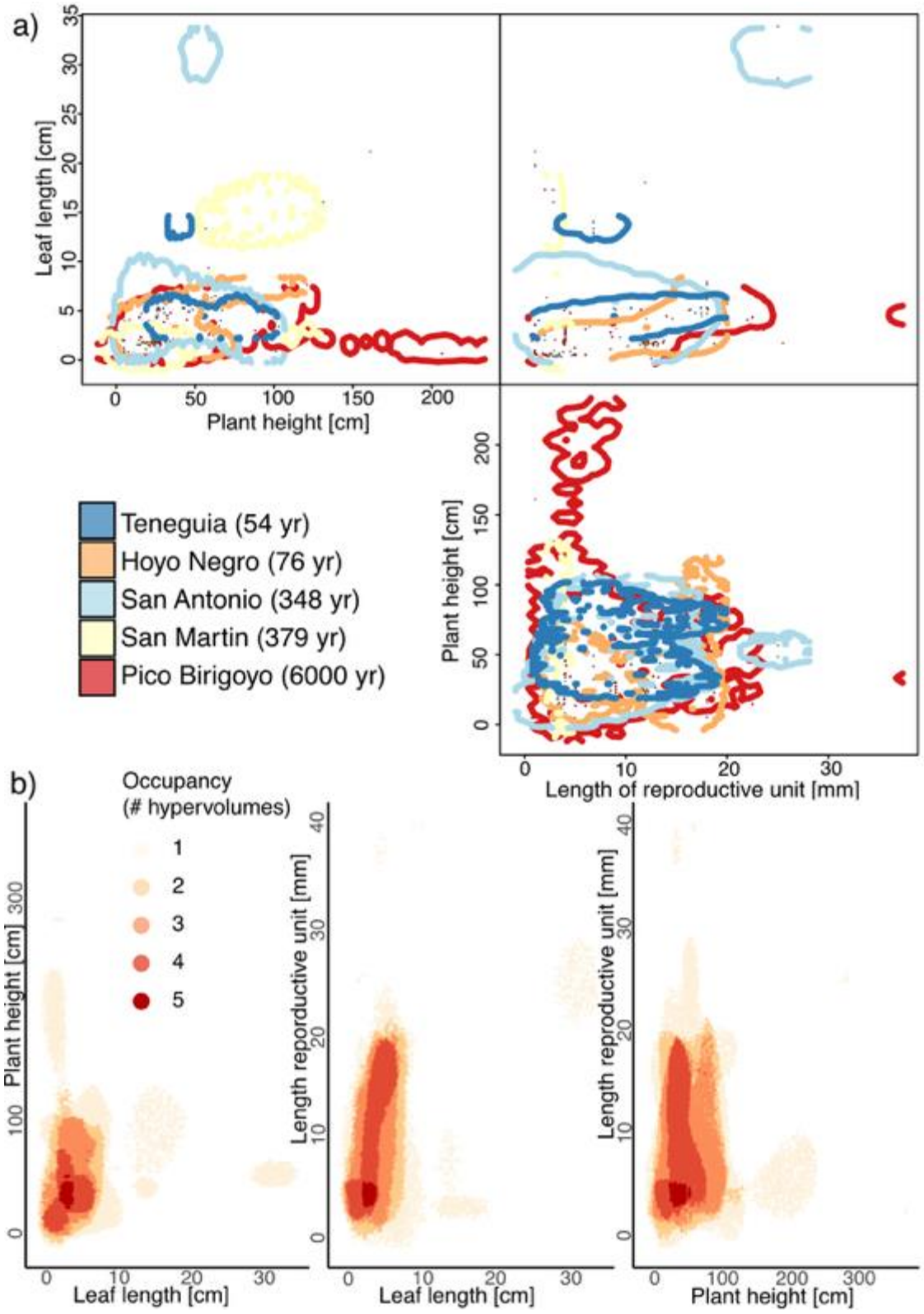

Figure 3. Differences in plant functional traits for the five tephra fields. (a) Estimated three-dimensional plant functional trait hypervolume based on a one-class support vector machine algorithm of the vegetation sampled on five aged tephra fields: Pico Birigoyo (n = 634 data

789 points), Hoyo Negro (n = 744 data points), San Martin (n = 179 data points), San Antonio (n =
790 224 data points), Teneguia (n = 115 data points). The small, coloured points represent the trait
791 data, whereas big, coloured points represent the centroids of the respective hypervolume. The
792 colored outline represents the area filled by Monte Carlo points sampled from the hypervolume.
793 The vegetation of Pico Birigoyo occupies the largest volume, whereas the vegetation on San
794 Martin occupies the smallest. (b) Occupied multidimensional trait space by the functional trait
795 hypervolumes of the five tephra fields. Shown here is the overlap of trait space occupied by
796 the hypervolumes. Most of the trait space is occupied by more than one hypervolume.

797

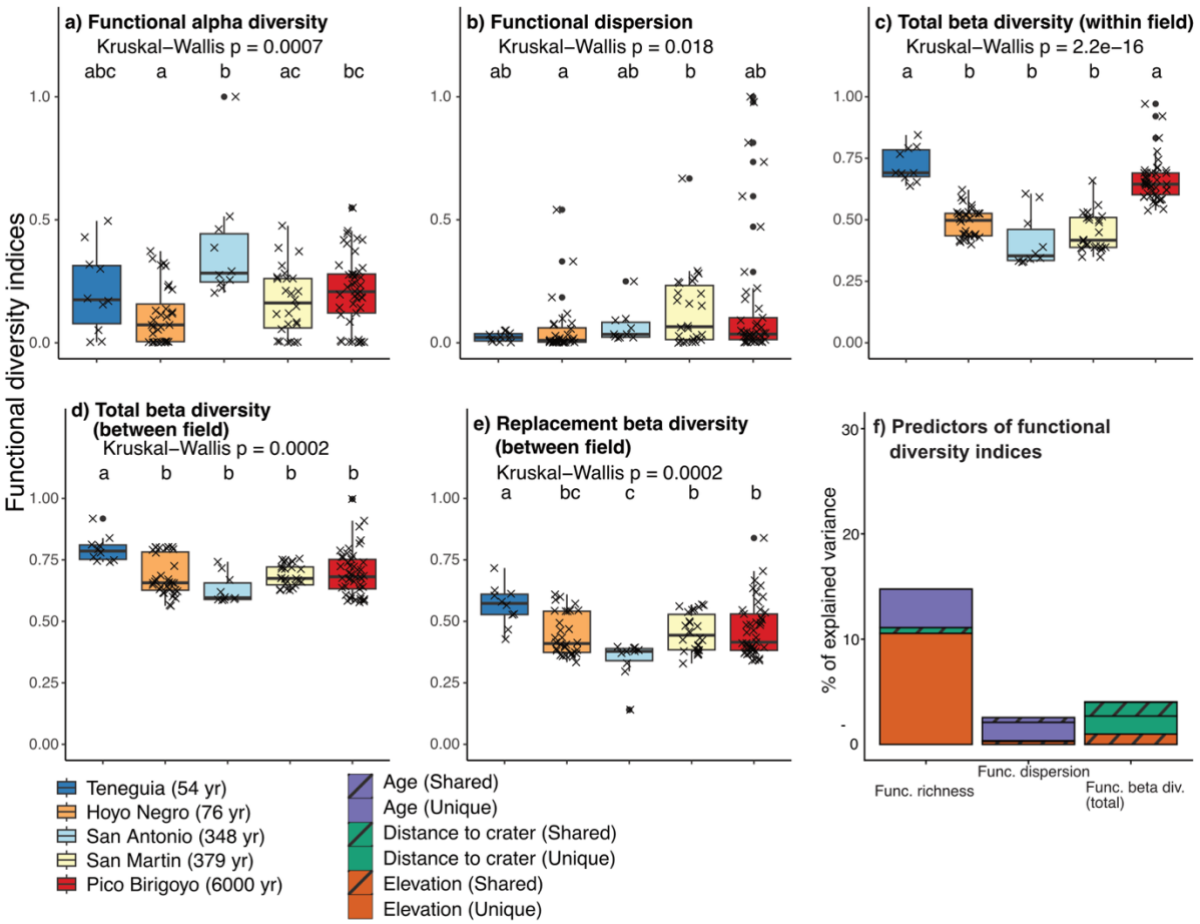

Figure 4. Differences in functional diversity indices between five tephra fields. (a) Functional richness (functional alpha diversity): significant differences across the fields are observed, with no clear trend. (b) Functional dispersion: dispersion is low, some significant differences are observed without a clear trend. (c) Total function beta diversity within each tephra field. The craters Hoyo Negro, San Antonio, and San Martin have a significant lower beta diversity than the youngest and oldest fields of Teneguia and Pico Birigoyo, respectively. (d) Total functional beta diversity is highest on Teneguia, with no clear trend towards the other craters. (e) Replacement beta diversity between the fields. The trend is similar to within-field functional beta diversity, however, less pronounced. Note that functional alpha diversity and functional dispersion were scaled between 0 and 1. (f) Relative contribution in abiotic predictors in explaining the observed variance in the functional diversity indices. Note that the unique (solid) and average shared (dashed) explained variance represent adjusted R^2 values.

Supplementary information

Supplementary methods

To create the phylogeny of the angiosperm species found on the studied tephra fields, we used an angiosperm phylogeny of the Canary Islands provided by [1] as a backbone. As not all species found on the tephra fields are included in this phylogeny, we opted to add the missing species using the function *phylo.maker()* with the scenario S3 (V.PhyloMaker2 package, [2]). The following species were added: *Rumex lunaria*, *Polycarpaea divaricata*, *Aeonium nobile*, *Polycarpaea aristata*, *Pterocephalus porphyranthus*, *Erica canariensis*, *Reseda luteola*, *Schizogyne sericea*, *Aeonium spathulatum*, *Rumex acetosella*, and *Tuberaria guttata*. *Pinus canariensis* could not be added to the angiosperm phylogeny and was removed from the analysis.

For species with unknown woodiness status, phylogenies and plant life forms (woody / herbaceous) were acquired from the literature and online herbaria. For *Euphorbia balsamifera* [3] and *Schizogyne sericea* [4], phylogenies were obtained from the literature. Sequences from *Pterocephalus porphyranthus* and of *Polycarpaea aristata* were not available. Therefore, genomic DNA was extracted from silica-dried leave samples collected during field work. Extraction and PCR amplification followed the methods described in [5]. The same primers (biomers.net GmbH, Ulm, Germany) were used for both PCR and Sanger sequencing and both strands were sequenced for all PCR products. For all regions, forward and reverse sequences were aligned with CodonCode Aligner v.3.0.3 (CodonCode Corp., Deham, Massachusetts, USA), and the consensus was exported in fasta format. For *Pterocephalus porphyranthus* and *Polycarpaea aristata,* the ITS4/ITS5m and c/f primers were used for sequencing. Sequencing was conducted by Eurofins Genomics (Ebersberg, Germany).

The newly created sequences were aligned with published sequences of the relevant related species, as acquired from the literature [6,7]. For *Schizogyne sericea*, *Bystropogon origanifolius*, *Polycarpaea divaricata* and *Polycarpaea aristata* all the sequences used to construct the original phylogeny were downloaded from GenBank. The phylogenetic tree of *Bystropogon origanifolius* was reconstructed based on ITS and ETS DNA-sequences [8]. For *Polycarpaea aristata* and *P. divaricata* the same approach was followed, with a reconstruction based on DNA sequences from plastid *rps16* and *ndhF*, as well as from nuclear ITS and RPB2 [7]. Alignments were conducted using MAFFT [9] with the –auto algorithm and a maximum-likelihood tree was estimated on the concatenated data matrices using IQTREE2 with ModelFinder to estimate the best DNA substitution model per gene alignment [10,11]. This was followed up by ancestral state estimations (see Methods).

For the species *Forsskaolea angustifolia* it was not possible to conduct an ancestral state reconstruction. Therefore, we used the phylogeny of [12] and a maximum parsimony approach (following [13]) to visually trace character evolution.

852 **Supplementary Tables**

853 **Supplement Table S1.** Life forms and ancestral or insular woodiness of the sampled species
854 in this study. Life forms were classified as woody or herbaceous as observed in the field.
855 Ancestral or insular woodiness of woody species was either obtained through literature or
856 through ancestral state reconstructions in this study.

Species	Woody / Herbaceous	Ancestral / Insular woody	Reference
Adenocarpus foliolosus (Aiton) DC., 1815	Woody	Ancestral	[14]
Aeonium davidbramwellii H.Y.Liu, 1989	Woody	Insular	[15]
Aeonium nobile (Praeger) Praeger, 1929	Woody	Insular	[15]
Aeonium spathulatum (Hornem.) Praeger, 1929	Woody	Insular	[15]
Argyranthemum webbii Sch.Bip., 1844	Woody	Insular	[15]
*Astydamia latifolia (*L.f.) Baill., 1879	Herbaceous	-	-
Bituminaria bituminosa (L.) C.H.Stirt., 1981	Woody	Insular	This study.
Bystropogon origanifolius L'Hér., 1789	Woody	Insular	This study.
Chamaecytisus proliferus (L.f.) Link, 1831	Woody	Ancestral	[16]
Cistus symphytifolius Lam., 1786	Woody	Ancestral	-
Descurainia gilva Svent., 1953	Woody	Insular	[15]

Echium brevirame Sprague & Hutch., 1914	Woody	Insular	[15]
Erica canariensis Rivas Mart., Martín Osorio & Wildpret, 2011	Woody	Ancestral	-
Euphorbia balsamifera Aiton, 1789	Woody	Derived [1)]	This study.
Forsskaolea angustifolia Retz., 1783	Woody	Ancestral	This study.
Hemionitis gluckuk Christenh., 2018	Herbaceous	-	-
Hypericum grandifolium Choisy, 1821	Woody	Ancestral	[17]
Kleinia neriifolia Haw., 1812	Woody	Derived [2)]	[18]
Limonium pectinatum (Aiton) Kuntze, 1891	Herbaceous [3)]	-	-
Logfia gallica (L.) Coss. & Germ., 1843	Herbaceous	-	-
Micromeria herpyllomorpha Webb & Berthel., 1844	Woody	Insular	[15]
Myrica faya Aiton, 1789	Woody	Ancestral	-
Pinus canariensis C.Sm. ex DC., 1828	Woody	Ancestral	-
Plantago webbii Barnéoud, 1845	Woody	Insular	[15]

Polycarpaea aristata (Aiton) C.Sm. ex DC., 1828	Woody	Ancestral	This study.
Polycarpaea divaricata (Aiton) Poir. ex Steud., 1841	Woody	Ancestral	This study.
Pteridium aquilinum (L.) Kuhn, 1879	Herbaceous	-	-
Pterocephalus porphyranthus Svent. (1969)	Woody	Derived [1)]	This study.
Reseda luteola L., 1753	Herbaceous	-	-
Rumex acetosella L., 1753	Herbaceous	-	-
Rumex lunaria L., 1753	Woody	Insular	[15]
Schizogyne sericea (L.f.) DC., 1836	Woody	Insular	This study.
Scrophularia glabrata Aiton, 1789	Herbaceous	-	-
Silene gallica L., 1753	Herbaceous	-	-
Silene vulgaris (Moench) Garcke, 1869	Herbaceous	-	-
Sonchus hierrensis (Pit.) Boulos, 1967	Woody	Insular	[15]
Tuberaria guttata (L.) Fourr., 1868	Herbaceous	-	-
Wahlenbergia lobelioides (L.f.) Link, 1829	Herbaceous	-	-

[1)] For *Euphorbia balsamifera* and *Pterocephalus porphyranthus*, the woodiness of these species evolved on the continent, meaning they are derived woody island species. In this study, we treat them in the same woody group as the ancestral woody species as they did not evolve their woodiness on an island.

[2)] For *Kleinia neriifolia*, no phylogeny containing this species could be obtained. Most of the continental relatives are woody and evolved their woodiness from herbaceous relatives, indicating a derived woodiness of this species.

[3)] For *Limonium pectinatum*, a woody base of the plant was observed. However, it did not extend to the upper stem parts, which means it did not satisfy our strict woodiness criteria (see Methods for details).

868 **Supplement Table S2.** Pairwise multilevel comparison for the Analysis of Similarities
869 (ANOSIM) for the plant communities observed on the five tephra fields. All p-values are $p <$
870 0.0009, meaning significant differences in community composition are observed between all
871 the craters.

Pair	***R* ANOSIM**	**p-value adjusted**
San Antonio – San Martin	0.380	0.00099
San Antonio – Pico Birigoyo	0.320	0.00099
San Antonio – Hoyo Negro	0.946	0.00099
San Antonio – Teneguia	0.498	0.00099
San Martin – Pico Birigoyo	0.250	0.00099
San Martin – Hoyo Negro	0.901	0.00099
San Martin – Teneguia	0.857	0.00099
Pico Birigoyo – Hoyo Negro	0.420	0.00099
Pico Birigoyo – Teneguia	0.612	0.00099
Hoyo Negro – Teneguia	0.980	0.00099

872

873

Supplement Table S3. Significance of predictors in explaining observed variance in (a) relative abundance of life forms, and in (b) functional diversity measures. Significance of predictors was assessed using permutation tests. Significiant predictors ($p < 0.05$) are written in bold.

Variable	Age	Distance to the crater	Elevation
a)			
Woody species	**0.018**	0.2627	0.6703
Herbaceous species	**0.018**	0.2488	0.6234
Insular woody species	**0.0001**	**0.0028**	0.23
Woody species with woody colonizers	**0.001**	**0.017**	0.29
b)			
Functional richness	0.067	0.31	**0.002**
Functional dispersion	0.052	0.73	0.49
Functional beta diversity (total)	0.59	**0.031**	0.14

Supplement Table S4. Pairwise multilevel comparison of overlap statistics of the Support-vector machine derived hypervolumes (SVM) of the vegetation on the respective tephra fields.

Comparison	Jaccard-Index	Unique fraction 1	Unique fraction 2	Jaccard p adjusted	Unique 1 p adjusted	Unique 2 p adjusted
PB – HN	0.202	0.784	0.252	< 0.0001	< 0.0001	1
PB – SM	0.028	0.971	0.549	< 0.0001	< 0.0001	0.04
PB – SA	0.388	0.472	0.406	1	1	0.29
PB – TG	0.223	0.770	0.125	0.05	0.05	1
HN – SM	0.056	0.935	0.708	0.01	0.01	0.05
HN – SA	0.140	0.501	0.838	0.75	1	< 0.0001
HN – TG	0.115	0.804	0.784	0.54	1	< 0.0001
SM – SA	0.020	0.716	0.979	< 0.0001	0.27	< 0.0001
SM – TG	0.005	0.976	0.994	< 0.0001	< 0.0001	< 0.0001
SA – TG	0.243	0.747	0.145	0.13	0.14	1

Supplement Table S5. Functional diversity indices and centroid location of the hypervolumes of the vegetation of the five aged tephra estimated using Gaussian kernel density estimation (KDE).

Tephra field	Functional richness	Functional dispersion	Centroid location – Leaf length [cm]	Centroid location – Plant height [cm]	Centroid location – Length reproducing unit [mm]
Pico Birigoyo	44041.8	67.1	3.63	41.83	9.85
Hoyo Negro	21015.1	37.4	1.79	22.28	13.28
San Martin	23960.5	65.97	4.56	40.05	3.38
San Antonio	37571.1	48.9	4.20	33.01	11.38
Teneguia	37118.5	46.5	6.01	44.66	11.18

Supplement Table S6. Pairwise multilevel comparison of overlap statistics of the Gaussian kernel density estimation derived hypervolumes of the vegetation on the respective tephra field.

Comparison	Jaccard-Index	Unique fraction 1	Unique fraction 2	Jaccard p adjusted	Unique 1 p adjusted	Unique 2 p adjusted
PB – HN	0.365	0.605	0.172	0	0	0.17
PB – SM	0.344	0.605	0.274	0	0	0.05
PB – SA	0.609	0.298	0.178	0	0.14	0.71
PB – TG	0.486	0.397	0.285	0	0.01	0.02
HN – SM	0.256	0.564	0.617	0	0	0
HN – SA	0.438	0.151	0.525	0	1	0
HN – TG	0.279	0.396	0.658	0	0.01	0
SM – SA	0.392	0.277	0.539	0	0.59	0
SM – TG	0.190	0.592	0.737	0	0	0
SA – TG	0.436	0.397	0.398	0	0.01	0

Supplementary Figures

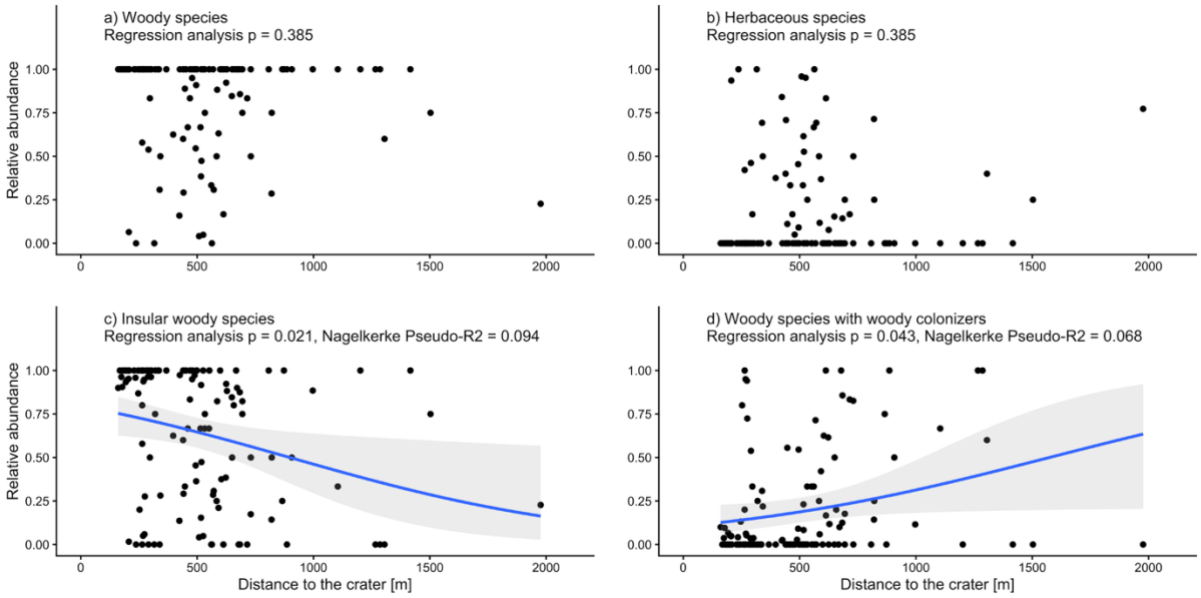

Supplement Figure S1. Relationship between distance and the abundance of (a) woody species, (b) herbaceous species, (c) insular woody species, and (d) woody species with woody colonizers.

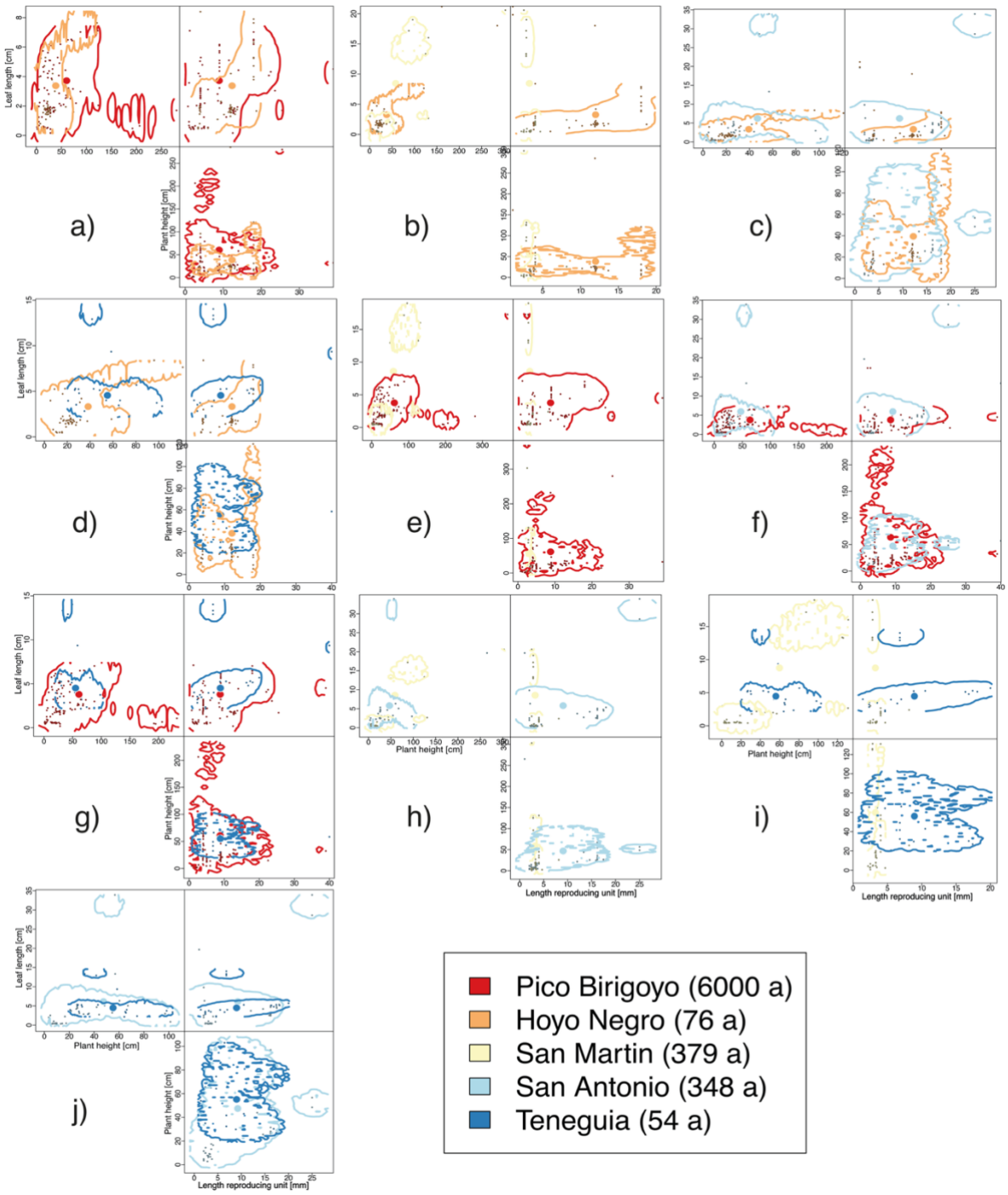

Supplement Figure S2. Pairwise comparison between the support-vector-machine derived hypervolumes (SVM).

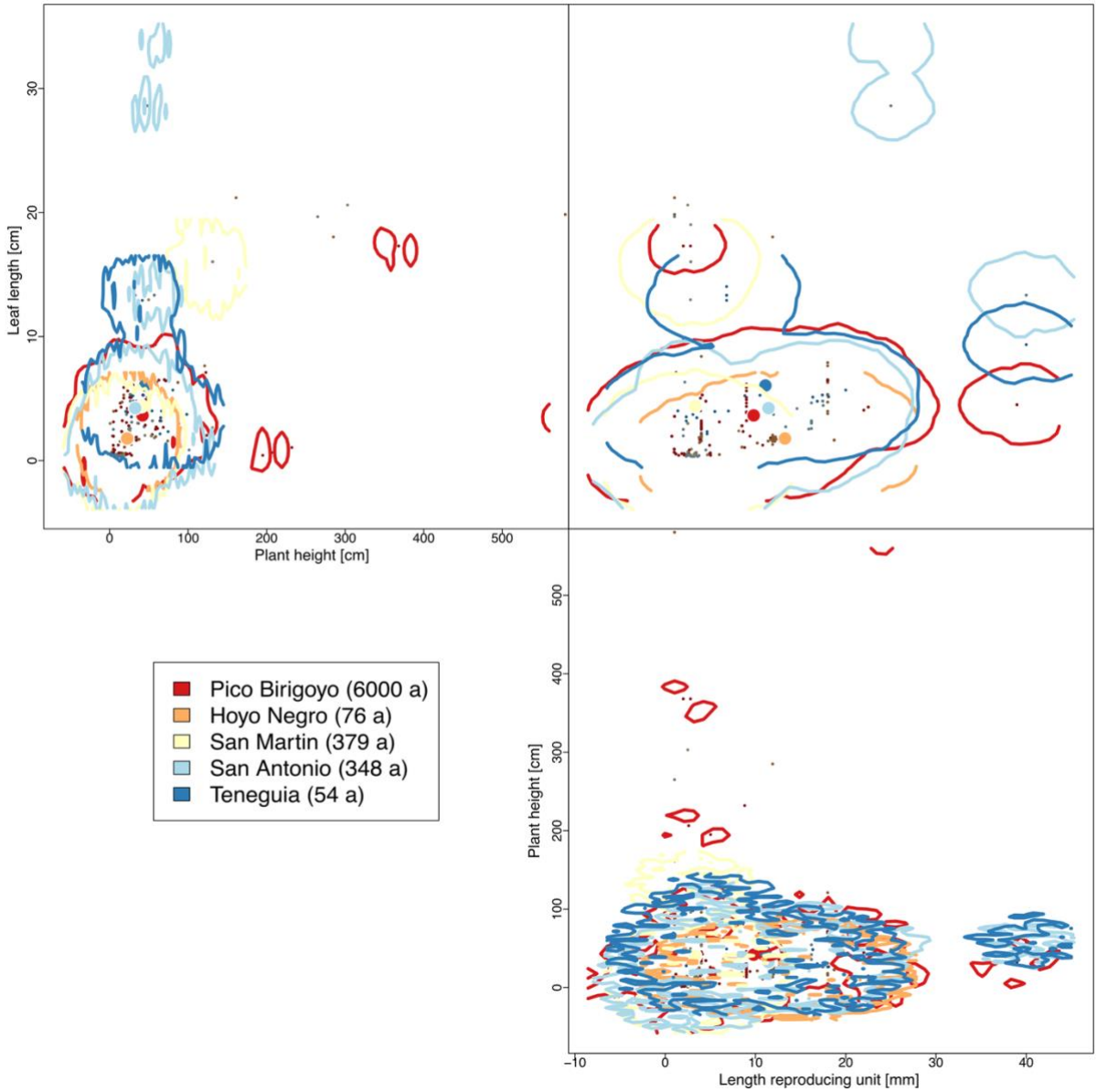

904

905 **Supplement Figure S3.** Differences in plant functional traits for the five tephra fields.
906 Estimated three-dimensional plant functional trait hypervolume based on Gaussian kernel
907 density estimation of the vegetation sampled on five aged tephra fields: Pico Birigoyo (n = 634
908 data points), Hoyo Negro (n = 744 data points), San Martin (n = 179 data points), San Antonio
909 (n = 224 data points), Teneguia (n = 115 data points). The small, colored points represent the
910 trait data, whereas big, colored points represent the centroids of the respective hypervolume.
911 The colored outline represents the area filled by Monte Carlo points sampled from the
912 hypervolume. The vegetation of Pico Birigoyo occupies the largest volume, whereas the
913 vegetation on San Martin the smallest.

914

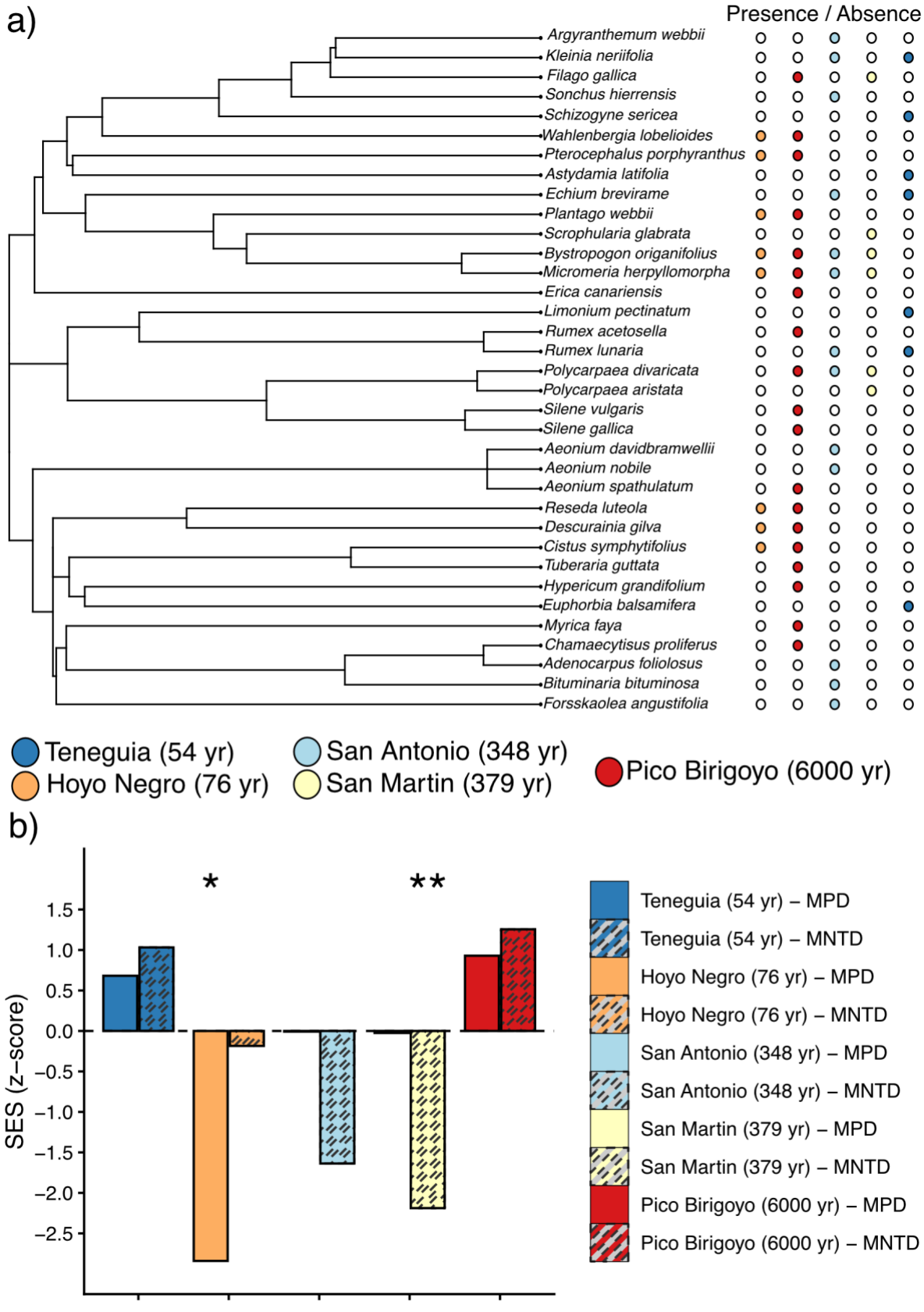

Supplement Figure S4. Phylogenetic relatedness and phylogenetic dispersion. (a) Phylogeny and occurrence of angiosperm species on the studied tephra fields. (b) Standard effect size (SES) of Mean Pairwise Distance (MPD) and Mean Nearest Taxon Distance (MNTD) of the tephra

field vegetation. Significant positive SES indicates phylogenetic overdispersion, whereas significant negative SES indicates phylogenetic clustering. Significance levels: *: $p \leq 0.05$, **: $p \leq 0.01$, ***: $p \leq 0.001$.

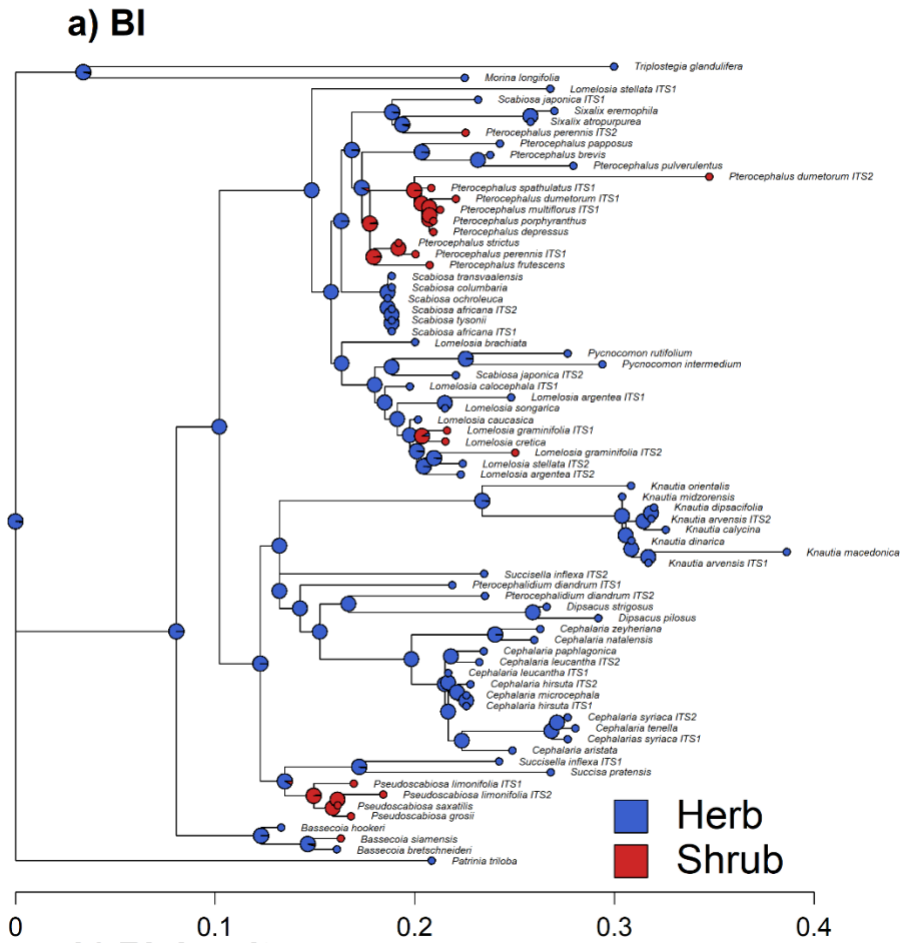
a) BI
Triplostegia glandulifera
Morina longifolia
Lomelosia stellata ITS1
Scabiosa japonica ITS1
Sixalix eremophila
Sixalix atropurpurea
Pterocephalus perennis ITS2
Pterocephalus papposus
Pterocephalus brevis
Pterocephalus pulverulentus
Pterocephalus dumetorum ITS2
Pterocephalus spathulatus ITS1
Pterocephalus dumetorum ITS1
Pterocephalus multiflorus ITS1
Pterocephalus porphyranthus
Pterocephalus depressus
Pterocephalus strictus
Pterocephalus perennis ITS1
Pterocephalus frutescens
Scabiosa transvaalensis
Scabiosa columbaria
Scabiosa ochroleuca
Scabiosa africana ITS2
Scabiosa lysonii
Scabiosa africana ITS1
Lomelosia brachiata
Pycnocomon rutifolium
Pycnocomon intermedium
Scabiosa japonica ITS2
Lomelosia calocephala ITS1
Lomelosia argentea ITS1
Lomelosia songarica
Lomelosia caucasica
Lomelosia graminifolia ITS1
Lomelosia cretica
Lomelosia graminifolia ITS2
Lomelosia stellata ITS2
Lomelosia argentea ITS2
Knautia orientalis
Knautia midzorensis
Knautia dipsacifolia
Knautia arvensis ITS2
Knautia calycina
Knautia dinarica
Knautia macedonica
Knautia arvensis ITS1
Succisella inflexa ITS2
Pterocephalidium diandrum ITS1
Pterocephalidium diandrum ITS2
Dipsacus strigosus
Dipsacus pilosus
Cephalaria zeyheriana
Cephalaria natalensis
Cephalaria paphlagonica
Cephalaria leucantha ITS2
Cephalaria leucantha ITS1
Cephalaria hirsuta ITS2
Cephalaria microcephala
Cephalaria hirsuta ITS1
Cephalaria syriaca ITS2
Cephalaria tenella
Cephalarias syriaca ITS1
Cephalaria aristata
Succisella inflexa ITS1
Succisa pratensis
Pseudoscabiosa limonifolia ITS1
Pseudoscabiosa limonifolia ITS2
Pseudoscabiosa saxatilis
Pseudoscabiosa grosii
Bassecoia hookeri
Bassecoia siamensis
Bassecoia bretschneideri
Patrinia triloba
Herb
Shrub
0
0.1
0.2
0.3
0.4

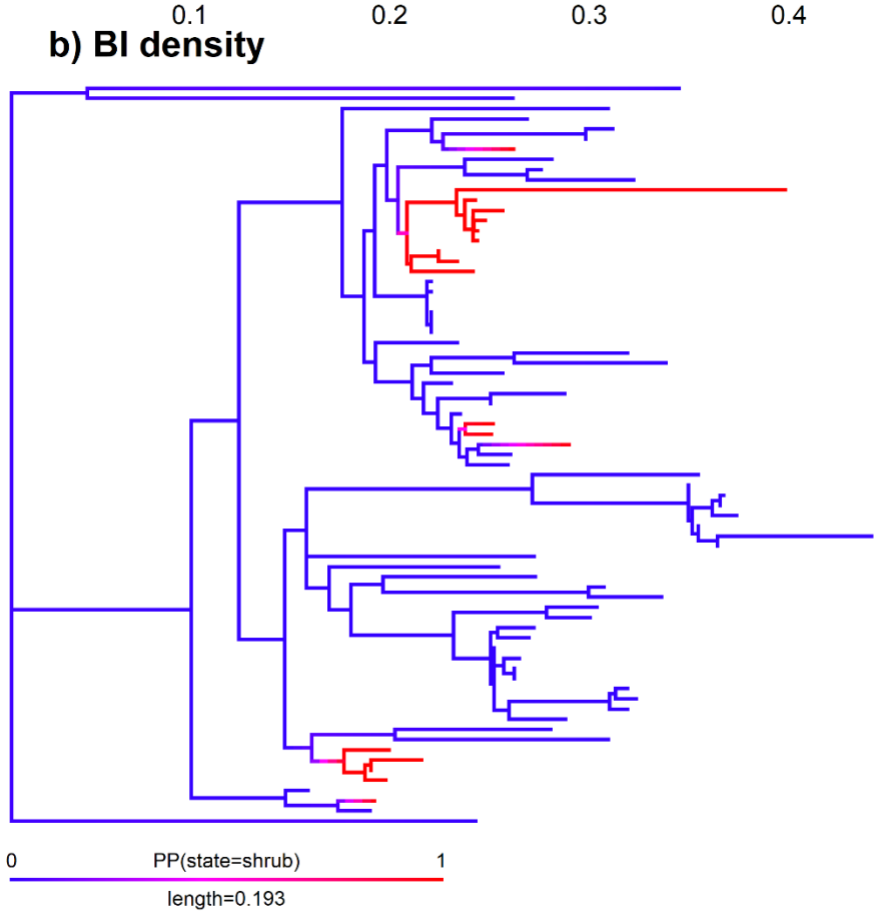
b) BI density
0
PP(state=shrub)
1
length=0.193

923

Supplement Figure S5. Ancestral state reconstruction of shrub (red) and herb (blue) lifeforms for the phylogenetic tree of Dipsacaceae (based on [6]). (a) Bayesian Inference (BI) of the phylogenetic tree of the Dipsacacaeae clade. The colored circles on the tree tips indicate the lifeform of the species (life form traits obtained from Plants of the World Online, Kew Gardens). Pie charts at the nodes represent the posterior probability of the ancestral state. (b) Bayesian inference (BI) density of the posterior probability plotted on the phylogenetic tree branches. In the Dipsacaceae tree used for the ancestral state reconstruction of *Pterocephalus porphyranthus* Svent., 1969, 7.952 life form changes between shrubs and herbs are reported on average. The transition herb to shrub occurred on average 6.811 times and the transition from shrub to herb on average 1.141 times. The species of interest, *Pterocephalus porphyranthus* is nested in a woody clade surrounded by herbaceous ancestors. Therefore, it is likely derived woody with ancestors that evolved woodiness on the continent and then spread to the Canaries. In this study this species is merged in the same woody group as the ancestral woody species, as it did not evolve its woodiness on an island.

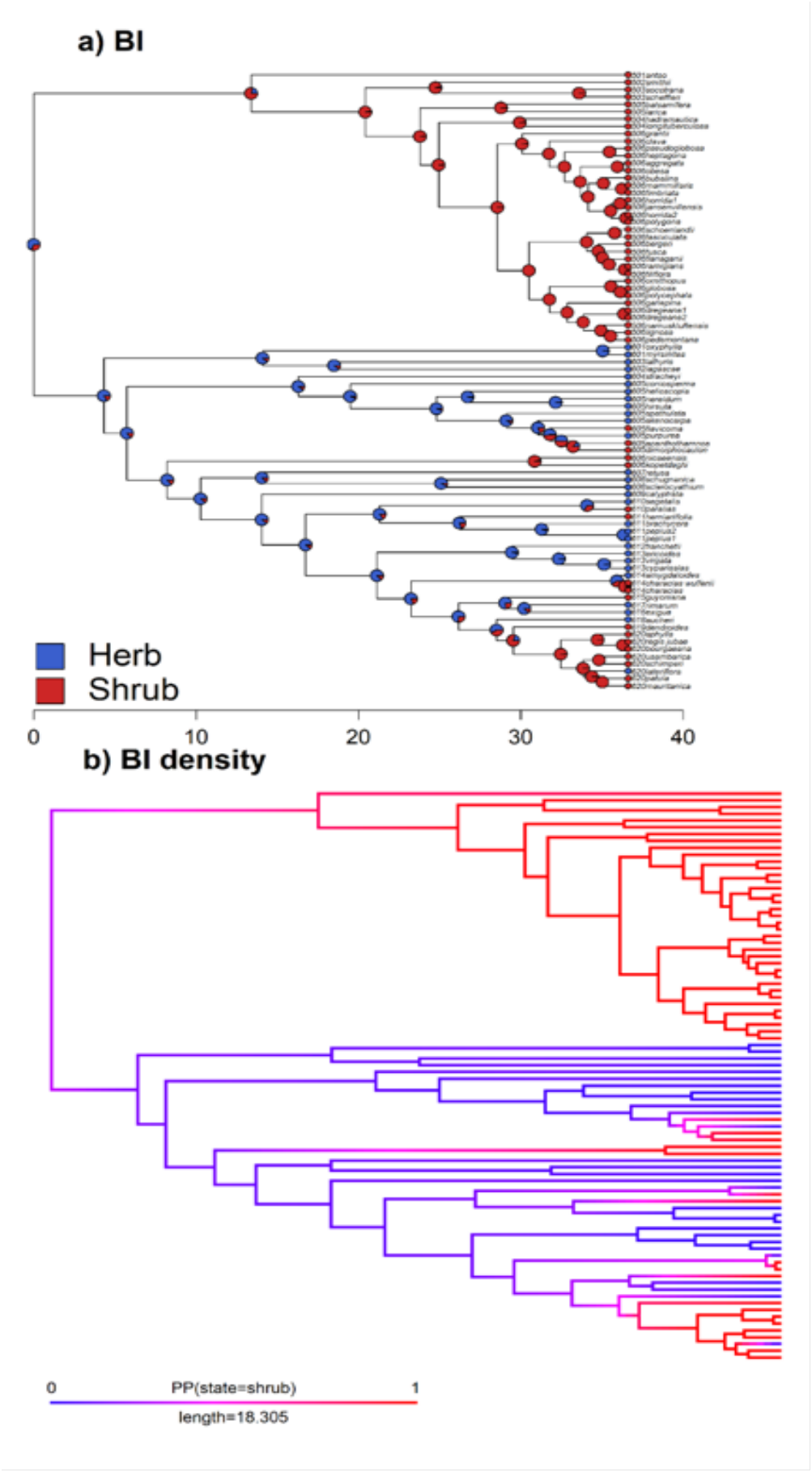
a) BI
Herb
Shrub
0
10
20
30
40
b) BI density
0
PP(state=shrub)
1
length=18.305

940

Supplement Figure S6. Ancestral state reconstruction of shrub (red) and herb (blue) lifeforms for the phylogenetic tree of *Euphorbia* (based on [3]). (a) Bayesian Inference (BI) of the phylogenetic tree of the *Euphorbia* clade. The colored circles on the tree tips indicate the lifeform of the species (life form traits obtained from Plants of the World Online, Kew Gardens). Pie charts at the nodes represent the posterior probability of the ancestral state. (b) Bayesian inference (BI) density of the posterior probability plotted on the phylogenetic tree branches. In the *Euphorbia* tree used for the ancestral state reconstruction of *Euphorbia balsamifera* Aiton, 1789, 20.415 life form changes between shrubs and herbs are reported on average. The transition from herb to shrub occurred on average 11.655 times and the transition shrub to herb on average 8.76 times. The species of interest, *Euphorbia balsamifera* is nested in a woody clade and its woodiness evolved on the continent. In this study this species is merged in the same woody group as the ancestral woody species, as it did not evolve its woodiness on an island.

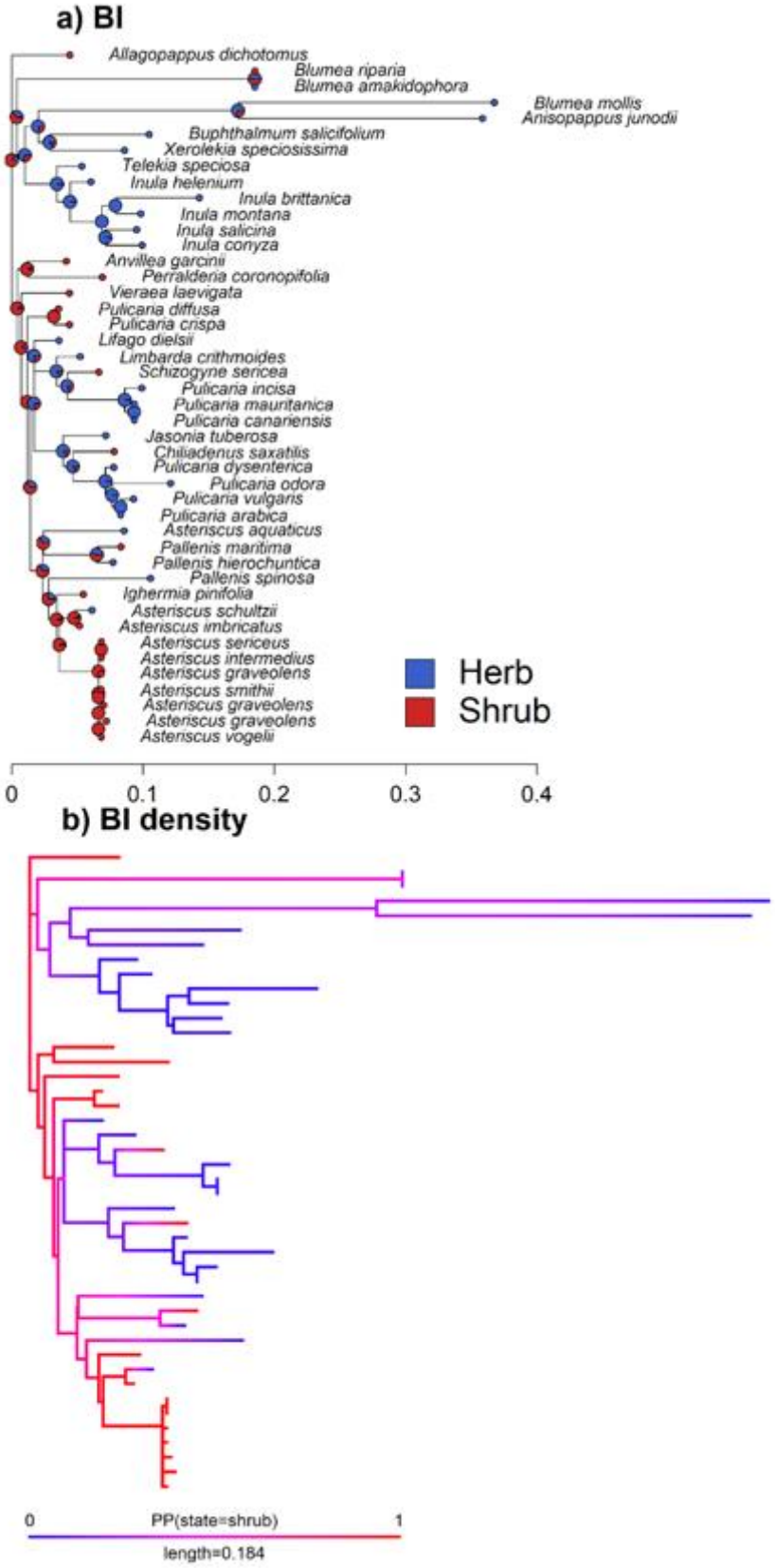

955

956 **Supplement Figure S7.** Ancestral state reconstruction of shrub (red) and herb (blue) lifeforms
957 for the phylogenetic tree of a subtree of the Inuleae tribe (*Asteraceae*) (based on [4]). (a) Bayesian

Inference (BI) of the phylogenetic tree of the Innuleae tribe. The coloured circles on the tree tips indicate the lifeform of the species (life form traits obtained from Plants of the World Online, Kew Gardens). Pie charts at the nodes represent the posterior probability of the ancestral state. (b) Bayesian inference (BI) density of the posterior probability plotted on the phylogenetic tree branches. In the Inuleae tribe used for the ancestral state reconstruction of *Schizogyne sericea* (L.f.) DC., 1836, 20.035 life form changes between shrubs and herbs are reported on average. The transition herb to shrub occurred on average 7.207 times and the transition shrub to herb on average 12.828 times. The species of interest, *Schizogyne sericea* is nested in a clade dominated by herbs and its closest relatives on the continent are herbaceous. Therefore, it is likely insular woody.

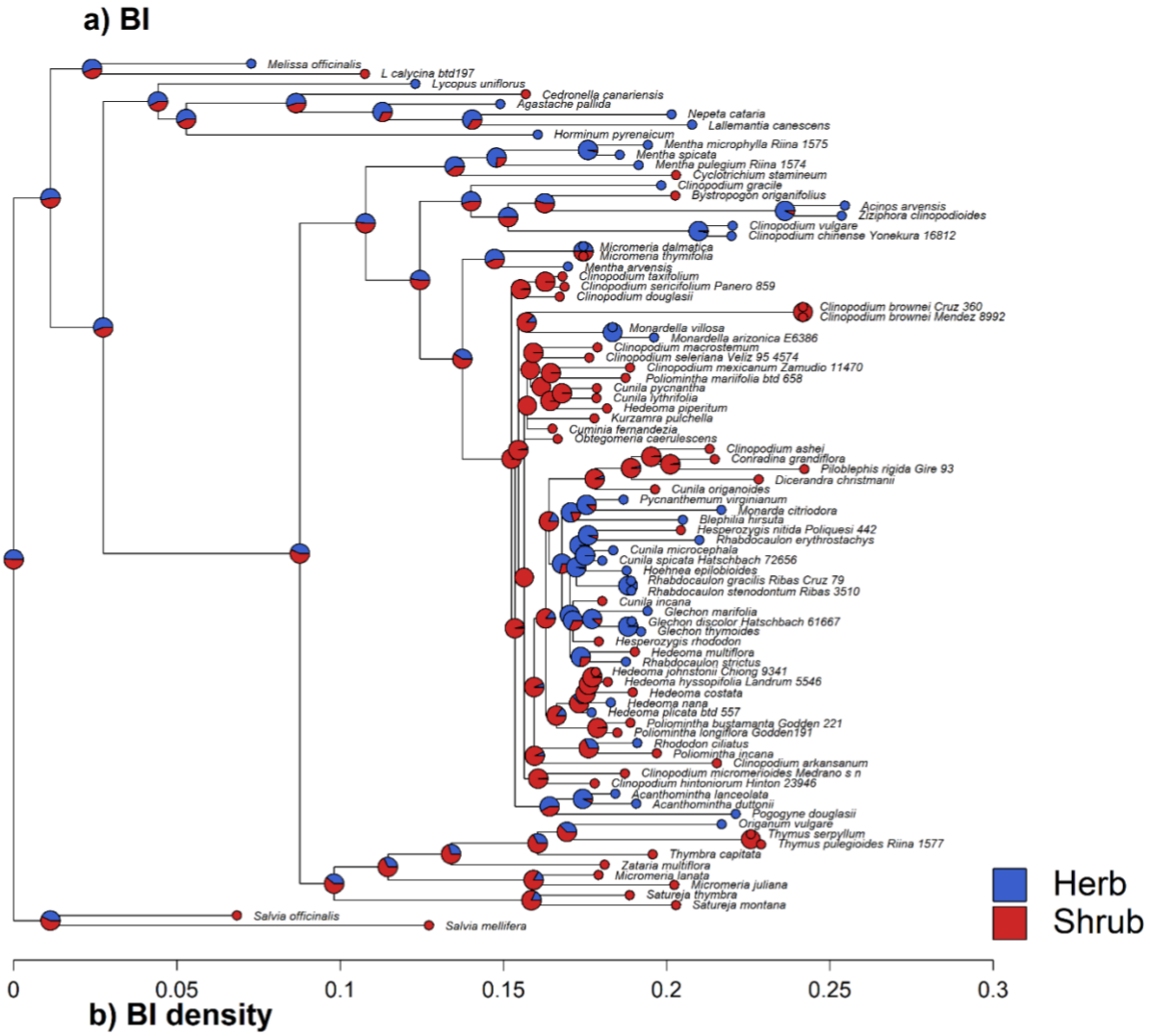
a) BI
Melissa officinalis
L calycina btd197
Lycopus uniflorus
Cedronella canariensis
Agastache pallida
Nepeta cataria
Lallemantia canescens
Horminum pyrenaicum
Mentha microphylla Riina 1575
Mentha spicata
Mentha pulegium Riina 1574
Cyclotrichium stamineum
Clinopodium gracile
Bystropogon origanifolius
Acinos arvensis
Ziziphora clinopodioides
Clinopodium vulgare
Clinopodium chinense Yonekura 16812
Micromeria dalmatica
Micromeria thymifolia
Mentha arvensis
Clinopodium taxifolium
Clinopodium sericeum Panero 859
Clinopodium douglasii
Clinopodium brownei Cruz 360
Clinopodium brownei Mendez 8992
Monardella villosa
Monardella arizonica E6386
Clinopodium macrostemum
Clinopodium seleriana Veliz 95 4574
Clinopodium mexicanum Zamudio 11470
Poliomintha mariifolia btd 658
Cunila pycnantha
Cunila lythrifolia
Hedeoma piperitum
Kurzamra pulchella
Cuminia fernandezia
Obtegomeria caerulescens
Clinopodium ashei
Conradina grandiflora
Piloblephis rigida Gire 93
Dicerandra christmanii
Cunila origanoides
Pycnanthemum virginianum
Monarda citriodora
Blephilia hirsuta
Hesperozygis nitida Poliquesi 442
Rhabdocaulon erythrostachys
Cunila microcephala
Cunila spicata Hatschbach 72656
Hoehnea epilobioides
Rhabdocaulon graciilis Ribas Cruz 79
Rhabdocaulon stenodontum Ribas 3510
Cunila incana
Glechon marifolia
Glechon discolor Hatschbach 61667
Glechon thymoides
Hesperozygis rhododon
Hedeoma multiflora
Rhabdocaulon strictus
Hedeoma johnstonii Chiong 9341
Hedeoma hyssopifolia Landrum 5546
Hedeoma costata
Hedeoma nana
Hedeoma plicata btd 557
Poliomintha bustamanta Godden 221
Poliomintha longiflora Godden191
Rhododon ciliatus
Poliomintha incana
Clinopodium arkansanum
Clinopodium micromerioides Medrano s n
Clinopodium hintoniorum Hinton 23946
Acanthomintha lanceolata
Acanthomintha duttonii
Pogogyne douglasii
Origanum vulgare
Thymus serpyllum
Thymus pulegioides Riina 1577
Thymbra capitata
Zataria multiflora
Micromeria lanata
Micromeria juliana
Satureja thymbra
Satureja montana
Salvia officinalis
Salvia mellifera
Herb
Shrub
0
0.05
0.1
0.15
0.2
0.25
0.3

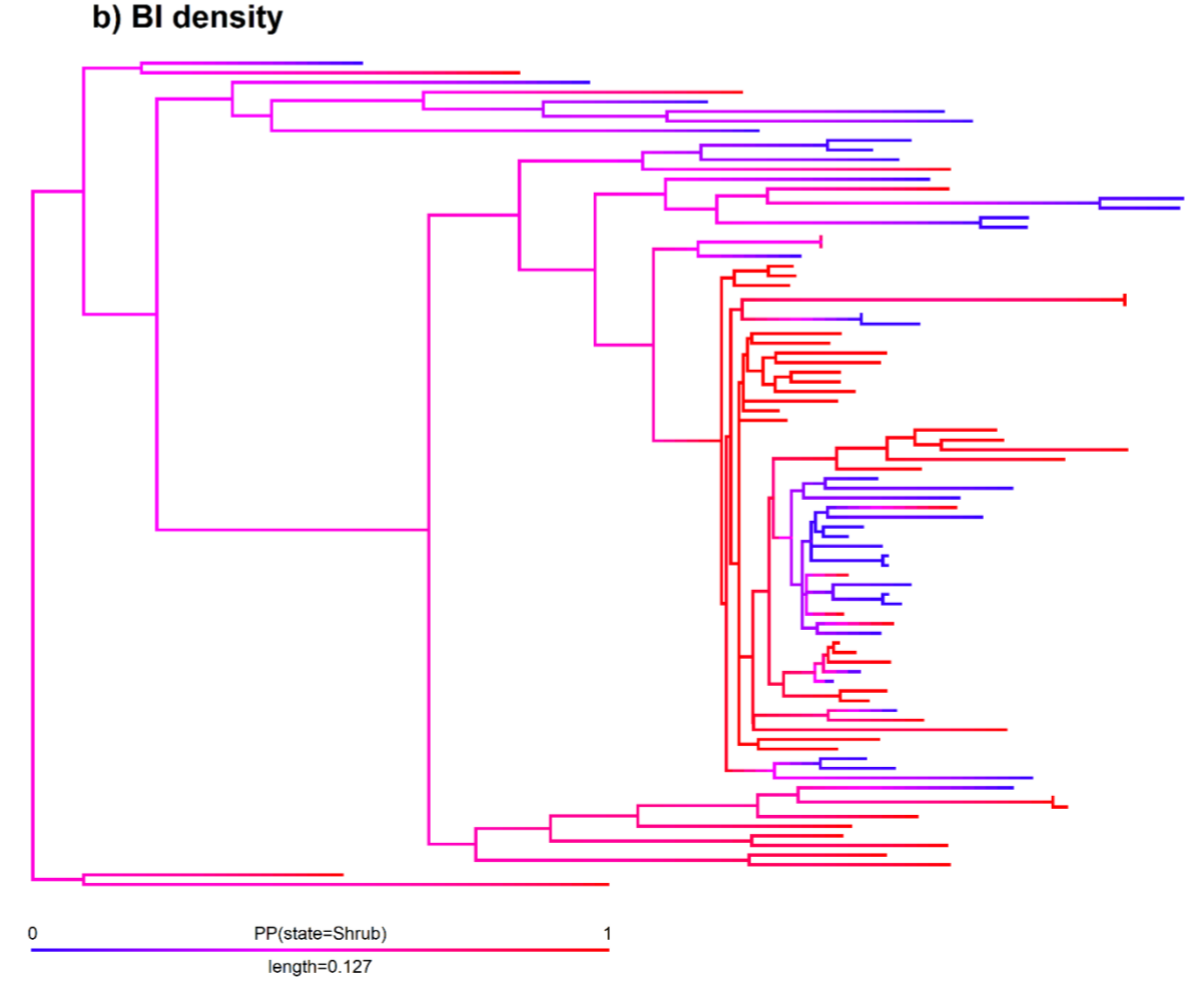
b) BI density
0
PP(state=Shrub)
1
length=0.127

Supplement Figure S8. Ancestral state reconstruction of shrub (red) or herb (blue) lifeforms of a subtree of the *Menthinae* (*Lamiaceae*) subtribe (based on [4]) (a) Bayesian inference (BI) of the phylogenetic tree of the *Menthinae* subtribe. The coloured circles on the tree tips indicate the lifeform of the species (lifeform traits obtained from Plants of the World Online, Kew Gardens: https://powo.science.kew.org/). Pie charts at the nodes represent the posterior probability of the ancestral state. (b) Bayesian inference (BI) density of the posterior probability plotted on the phylogenetic tree branches. In the Menthinae (Lamiaceae) subtree used for the ancestral state reconstruction of *Bystropogon origanifolius* L'Hér., 1789, 53.407 life form changes between shrubs and herbs are reported on average. The transition herb to shrub occurred on average 25.213 times, whereas the transition from shrub to herb was more frequent, occurring on average 28.194 times. The species of interest, *Bystropogon origanifolius* L'Hér., 1789, evolved woodiness in a clade with high abundance of herbaceous species and can therefore be seen as insular woody.

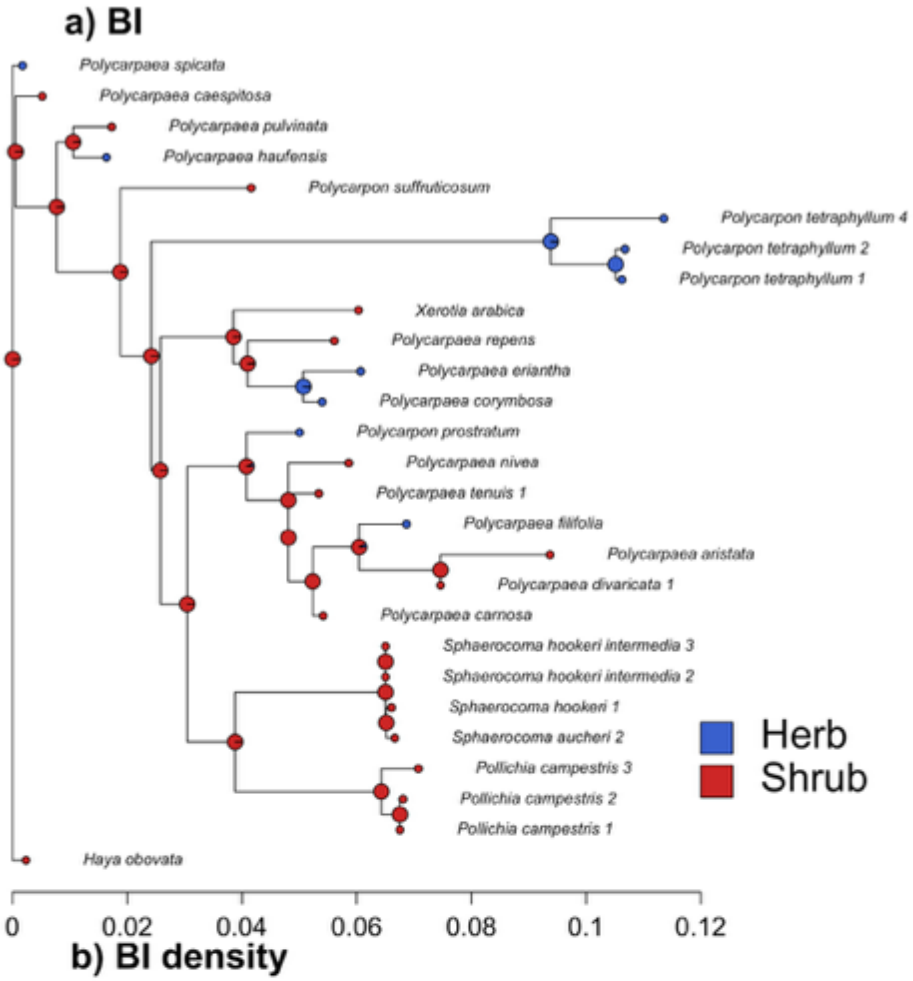
a) BI
Polycarpaea spicata
Polycarpaea caespitosa
Polycarpaea pulvinata
Polycarpaea haufensis
Polycarpon sulfruticosum
Polycarpon tetraphyllum 4
Polycarpon tetraphyllum 2
Polycarpon tetraphyllum 1
Xerotia arabica
Polycarpaea repens
Polycarpaea eriantha
Polycarpaea corymbosa
Polycarpon prostratum
Polycarpaea nivea
Polycarpaea tenuis 1
Polycarpaea filifolia
Polycarpaea aristata
Polycarpaea divaricata 1
Polycarpaea carnosa
Sphaerocoma hookeri intermedia 3
Sphaerocoma hookeri intermedia 2
Sphaerocoma hookeri 1
Sphaerocoma aucheri 2
Pollichia campestris 3
Pollichia campestris 2
Pollichia campestris 1
Haya obovata
Herb
Shrub
0
0.02
0.04
0.06
0.08
0.1
0.12

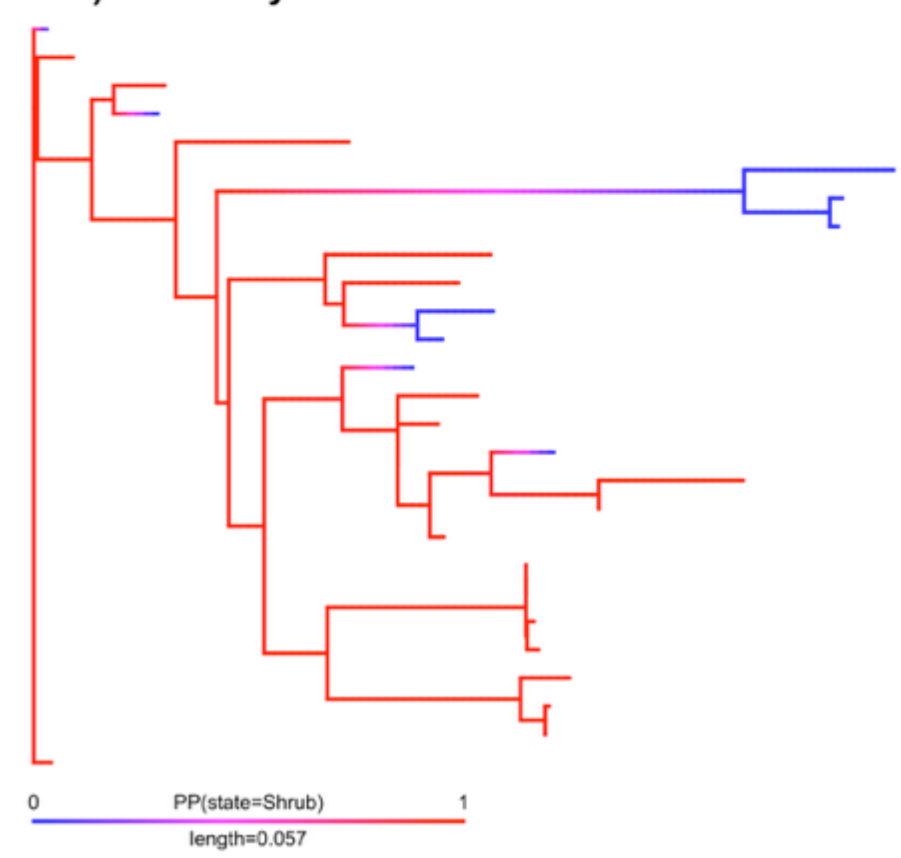
b) BI density
0
PP(state=Shrub)
1
length=0.057

984

Supplement Figure S9. Ancestral state reconstruction of shrub (red) or herb (blue) lifeforms of a subclade of the genus *Polycarpaea* (*Caryophyllaceae*) (based on [7]). (a) Bayesian inference (BI) of the phylogenetic tree of the *Polycarpaea* genus. The coloured circles on the tree tips indicate the lifeform of the species (lifeform traits obtained from Plants of the World Online, Kew Gardens: https://powo.science.kew.org/). Pie charts at the nodes represent the posterior probability of the ancestral state. (b) Bayesian inference (BI) density of the posterior probability plotted on the phylogenetic tree branches. In *Polycarpaea* (Caryophyllaceae) subtree used for the ancestral state reconstruction of *Polycarpaea divaricata* (Aiton) Poir. ex Steud., 1841, and *Polycarpaea aristata* (Aiton) C.Sm. ex DC., 1828, on average 6.436 life form changes between shrubs and herbs are reported. The transition from herb to shrub occurred on average 0.322 times, whereas the transition from shrub to herb occurred 6.114 times on average. The species of interest, *Polycarpaea divaricata* (Aiton) Poir. ex Steud., 1841, and *Polycarpaea aristata* (Aiton) C.Sm. ex DC., 1828, and all other Canary *Polycarpaea* species are located in a clade with a high posterior probability of being woody. Therefore, these species are most likely ancestral woody.

Supplement References

1. Brewer, R. F. A. et al. Trait-dependent diversification and spatio-ecological limits drive angiosperm diversity unevenness across the Canary Islands archipelago. 2025.09.19.677265 Preprint at https://doi.org/10.1101/2025.09.19.677265 (2025).
2. Jin, Y. & Qian, H. V.PhyloMaker2: an updated and enlarged R package that can generate very large phylogenies for vascular plants. *Plant Divers.* **44**, 335–339 (2022).
3. Coello, A. J., Vargas, P., Cano, E., Riina, R. & Fernández-Mazuecos, M. Phylogenetics and phylogeography of Euphorbia canariensis reveal an extreme Canarian-Asian disjunction but limited inter-island colonization. *Plant Biol.* **26**, 398–414 (2024).
4. Francisco-Ortega, J., Park, S.-J., Santos-guerra, A., Benabid, A. & Jansen, R. K. Origin and evolution of the endemic Macaronesian Inuleae (Asteraceae): evidence from the internal transcribed spacers of nuclear ribosomal DNA. *Biol. J. Linn. Soc.* **72**, 77–97 (2001).
5. Liede-Schumann, S. & Meve, U. The Orthosiinae revisited (Apocynaceae, Asclepiadoideae, Asclepiadeae). *Ann. Mo. Bot. Gard.* **99**, 44–81 (2013).
6. Carlson, S. E., Mayer, V. & Donoghue, M. J. Phylogenetic relationships, taxonomy, and morphological evolution in Dipsacaceae (Dipsacales) inferred by DNA sequence data. *TAXON* **58**, 1075–1091 (2009).
7. Kool, A., Perrigo, A. & Thulin, M. Bristly versus juicy: phylogenetic position and taxonomy of Sphaerocoma (Caryophyllaceae). *TAXON* **61**, 67–75 (2012).
8. Drew, B. T., Liu, S., Bonifacino, J. M. & Sytsma, K. J. Amphitropical disjunctions in New World Menthinae: three Pliocene dispersals to South America following late Miocene dispersal to North America from the Old World. *Am. J. Bot.* **104**, 1695–1707 (2017).
9. Katoh, K. & Standley, D. M. MAFFT Multiple Sequence Alignment Software Version 7: improvements in performance and usability. *Mol. Biol. Evol.* **30**, 772–780 (2013).
10. Kalyaanamoorthy, S., Minh, B. Q., Wong, T. K. F., von Haeseler, A. & Jermiin, L. S. ModelFinder: fast model selection for accurate phylogenetic estimates. *Nat. Methods* **14**, 587–589 (2017).
11. Minh, B. Q. *et al.* IQ-TREE 2: new models and efficient methods for phylogenetic inference in the genomic era. *Mol. Biol. Evol.* **37**, 1530–1534 (2020).
12. Wu, Z.-Y. *et al.* Testing Darwin's transoceanic dispersal hypothesis for the inland nettle family (Urticaceae). *Ecol. Lett.* **21**, 1515–1529 (2018).
13. Zizka, A. *et al.* The evolution of insular woodiness. *Proc. Natl. Acad. Sci.* **119**, e2208629119 (2022).

14. Cubas, P., Pardo, C., Tahiri, H. & Castroviejo, S. Phylogeny and evolutionary diversification of Adenocarpus DC. (Leguminosae). *Taxon* **59**, 720–732 (2010).
15. Hooft van Huysduynen, A. *et al.* Temporal and palaeoclimatic context of the evolution of insular woodiness in the Canary Islands. *Ecol. Evol.* **11**, 12220–12231 (2021).
16. Cubas, P., Pardo, C. & Tahiri, H. Molecular approach to the phylogeny and systematics of Cytisus (Leguminosae) and related genera based on nucleotide sequences of nrDNA (ITS region) and cpDNA (trnL-trnF intergenic spacer). *Plant Syst. Evol.* **233**, 223–242 (2002).
17. Nürk, N. M., Madriñán, S., Carine, M. A., Chase, M. W. & Blattner, F. R. Molecular phylogenetics and morphological evolution of St. John's wort (*Hypericum*; Hypericaceae). *Mol. Phylogenet. Evol.* **66**, 1–16 (2013).
18. Lens, F., Davin, N., Smets, E. & del Arco, M. Insular woodiness on the Canary Islands: a remarkable case of convergent evolution. *Int. J. Plant Sci.* **174**, 992–1013 (2013).